2001, 2003). Oyake et al. (2002) developed double RING ubiquitin ligases containing the RING finger domains of both BRCA and BARD1 linked to a substrate recognition site PCNA. Recently, Hatakeyama et al. developed a fusion protein composed of Max, which forms a heterodimer with c-Myc, and the U-box of CHIP. This fusion protein physically interacted with c-Myc and promoted the ubiquitylation of c-Myc. It also reduced the stability of c-Myc, resulting in the suppression of transcriptional activity dependent on c-Myc and the inhibition of tumorogenesis (Hatakeyama et al., 2005). This indicated that the U-box portion of CHIP is able to add an effective E3 function to a U-box-containing client protein.

We postulated that engineered forms of Dorfin could be stable and still function as specific E3s for mutant SOD1s. Dorfin has a RING/IBR domain in the N-terminal portion (amino acids 1-332), but has no obvious motif in the rest of the C-terminus (amino acids 333–838). In this study, we have demonstrated that the hydrophobic domain of Dorfin (amino acids 333–454) is both necessary and sufficient for substrate recruiting (Fig. 2B). In our engineered proteins, the RING/IBR motif of N-terminal Dorfin was replaced by the UPR domain of CHIP, which had strong E3 activity (Murata et al., 2001). Some of the engineered Dorfin-chimeric proteins, such as Dorfin-CHIP$^{D, G, J}$, and ^{L}, were degraded *in vivo* far more slowly than was wild-type Dorfin, indicating that they were capable of being stably presented *in vivo* (Fig. 3). However, Dorfin-CHIP^{G} failed to show strong ubiquitylation activity against SOD1^{G85R} in HEK293 cells. Since Dorfin-CHIP$^{D, J}$, and ^{L} were able to bind to SOD1^{G85R} more strongly than did Dorfin-CHIP^{G}, the binding activity was more important for the E3 activity than for the protein stability.

We next showed that although all of the Dorfin-CHIP chimeric proteins bound to mutant SOD1 *in vivo*, some of them, such as Dorfin-CHIP$^{B, C}$, and ^{I}, bound less than others (Fig. 4A). In HEK293 cells, Dorfin-CHIP$^{D, E, F, J, K}$, and ^{L} ubiquitylated SOD1^{G85R} more effectively than did Dorfin or CHIP; however, in N2a cells only Dorfin-CHIP^{L} had more effective E3 activity than did Dorfin or CHIP. This discrepancy may be due to differences between HEK 293 and N2a cells which could provide slight different environment for the E3 machinery. Therefore, Dorfin-CHIP^{L} was the most potent of the candidate chimeric proteins in degrading mutant SOD1 in the UPS in neuronal cells. We also showed that Dorfin-CHIP^{L} could specifically bind to and ubiquitylate mutant SOD1s but not SOD1^{WT} *in vivo*, as Dorfin had done (Niwa et al., 2002; Ishigaki et al., 2004) (Fig. 5). This observation confirmed that the hydrophobic domain of Dorfin (amino acids 333–454) is responsible for mutant SOD1 recruiting.

Pulse-chase analysis using N2a cells showed that Dorfin-CHIP^{L} degraded SOD1^{G85R} and SOD1^{G93A} more effectively than did Dorfin (Fig. 6). This is compatible with the finding that Dorfin-CHIP^{L} had a greater effect than Dorfin did on the ubiquitylation against mutant SOD1. The cycloheximide assay verified that the degradation ability of Dorfin-CHIP^{L} against SOD1^{G85R} was stronger than that of Dorfin or CHIP in HEK293 cells (data not shown).

Dorfin-CHIP^{L} also reversed SOD1^{G85R}-associated toxicity in N2a cells more effectively than did Dorfin (Fig. 7). This therapeutic effect of Dorfin-CHIP^{L} was expected from its strong E3 activity and degradation ability against SOD1^{G85R}. Visible protein aggregations have been considered to be hallmarks of neurodegeneration. Increased understanding of the pathway involved in protein aggregation may demonstrate that visible macroaggregates represent the end-stage of a molecular cascade of steps rather than a direct toxic insult (Ross and Poirier, 2004). Two facts that Dorfin-CHIP^{L} decreased aggregation formation of SOD1^{G85R} and that this effect was inhibited by a proteasome inhibitor should reflect the ability of Dorfin-CHIP^{L} to degrade mutant SOD1 in the UPS of cells.

Based on our present observations, Dorfin-CHIP^{L}, an engineered chimeric molecule with the hydrophobic substrate-binding domain of Dorfin and the U-box domain of CHIP, had stronger E3 activity against mutant SOD1 than did Dorfin or CHIP. Indeed, it not only degraded mutant SOD1 more effectively than did Dorfin or CHIP but, as compared to Dorfin, produced marked attenuation of mutant SOD1-associated toxicity in N2a cells. This protective effect of Dorfin-CHIP^{L} against mutant SOD1 has potential applications to gene therapy for mutant SOD1 transgenic mice because this protein has a long enough life to allow the constant removal of mutant SOD1 from neurons. Since Dorfin was originally identified as a sporadic ALS-associated molecule (Ishigaki et al., 2002b) and is located in the ubiquitin-positive inclusions of various neurodegenerative diseases (Hishikawa et al., 2003), this molecule is an appropriate candidate for future use in gene therapy not only for familial ALS, but also for sporadic ALS and other neurodegenerative disorders.

So far, most reports on engineered chimera E3s have targeted cancer-promoting proteins. Dorfin-CHIP chimeric proteins are the first chimera E3s to be intended for the treatment of neurodegenerative diseases. Since the accumulation of ubiquitylated proteins in neurons is a pathological hallmark of various neurodegenerative diseases, development of chimera E3s like Dorfin-CHIP^{L}, which can remove unnecessary proteins, is a new therapeutic concept. Further analysis, including transgenic overexpression and vector delivery of Dorfin-CHIP chimeric proteins using ALS animal models will increase our understanding of the potential utility of Dorfin-CHIP chimeric proteins as therapeutic tools.

Acknowledgments

We gratefully thank Dr. Shigetsugu Hatakeyama at Hokkaido University for his advice about the construction of Dorfin-CHIP chimeric proteins. This work was supported by the Nakabayashi Trust for ALS Research; a grant for Center of Excellence (COE) from the Ministry of Education, Culture, Sports, Science and Technology of Japan; and grants from the Ministry of Health, Welfare and Labor of Japan.

Appendix A. Supplementary data

Supplementary data associated with this article can be found, in the online version, at doi:10.1016/j.nbd.2006.09.017.

References

Alves-Rodrigues, A., Gregori, L., Figueiredo-Pereira, M.E., 1998. Ubiquitin, cellular inclusions and their role in neurodegeneration. Trends Neurosci. 21, 516–520.

Bercovich, B., Stancovski, I., Mayer, A., Blumenfeld, N., Laszlo, A., Schwartz, A.L., Ciechanover, A., 1997. Ubiquitin-dependent degradation of certain protein substrates in vitro requires the molecular chaperone Hsc70. J. Biol. Chem. 272, 9002–9010.

Ciechanover, A., Brundin, P., 2003. The ubiquitin proteasome system in

neurodegenerative diseases: sometimes the chicken, sometimes the egg. Neuron 40, 427–446.

Cudkowicz, M.E., McKenna-Yasek, D., Sapp, P.E., Chin, W., Geller, B., Hayden, D.L., Schoenfeld, D.A., Hosler, B.A., Horvitz, H.R., Brown, R.H., 1997. Epidemiology of mutations in superoxide dismutase in amyotrophic lateral sclerosis. Ann. Neurol. 41, 210–221.

Glickman, M.H., Ciechanover, A., 2002. The ubiquitin–proteasome proteolytic pathway: destruction for the sake of construction. Physiol. Rev. 82, 373–428.

Hatakeyama, S., Matsumoto, M., Kamura, T., Murayama, M., Chui, D.H., Planel, E., Takahashi, R., Nakayama, K.I., Takashima, A., 2004. U-box protein carboxyl terminus of Hsc70-interacting protein (CHIP) mediates poly-ubiquitylation preferentially on four-repeat Tau and is involved in neurodegeneration of tauopathy. J. Neurochem. 91, 299–307.

Hatakeyama, S., Watanabe, M., Fujii, Y., Nakayama, K.I., 2005. Targeted destruction of c-Myc by an engineered ubiquitin ligase suppresses cell transformation and tumor formation. Cancer Res. 65, 7874–7879.

Hishikawa, N., Niwa, J., Doyu, M., Ito, T., Ishigaki, S., Hashizume, Y., Sobue, G., 2003. Dorfin localizes to the ubiquitylated inclusions in Parkinson's disease, dementia with Lewy bodies, multiple system atrophy, and amyotrophic lateral sclerosis. Am. J. Pathol. 163, 609–619.

Ishigaki, S., Liang, Y., Yamamoto, M., Niwa, J., Ando, Y., Yoshihara, T., Takeuchi, H., Doyu, M., Sobue, G., 2002a. X-Linked inhibitor of apoptosis protein is involved in mutant SOD1-mediated neuronal degeneration. J. Neurochem. 82, 576–584.

Ishigaki, S., Niwa, J., Ando, Y., Yoshihara, T., Sawada, K., Doyu, M., Yamamoto, M., Kato, K., Yotsumoto, Y., Sobue, G., 2002b. Differentially expressed genes in sporadic amyotrophic lateral sclerosis spinal cords—Screening by molecular indexing and subsequent cDNA microarray analysis. FEBS Lett. 531, 354–358.

Ishigaki, S., Hishikawa, N., Niwa, J., Iemura, S., Natsume, T., Hori, S., Kakizuka, A., Tanaka, K., Sobue, G., 2004. Physical and functional interaction between Dorfin and Valosin-containing protein that are colocalized in ubiquitylated inclusions in neurodegenerative disorders. J. Biol. Chem. 279, 51376–51385.

Ito, T., Niwa, J., Hishikawa, N., Ishigaki, S., Doyu, M., Sobue, G., 2003. Dorfin localizes to Lewy bodies and ubiquitylates synphilin-1. J. Biol. Chem. 278, 29106–29114.

Johnston, J.A., Ward, C.L., Kopito, R.R., 1998. Aggresomes: a cellular response to misfolded proteins. J. Cell Biol. 143, 1883–1898.

Julien, J.P., 2001. Amyotrophic lateral sclerosis. unfolding the toxicity of the misfolded. Cell 104, 581–591.

Jungmann, J., Reins, H.A., Schobert, C., Jentsch, S., 1993. Resistance to cadmium mediated by ubiquitin-dependent proteolysis. Nature 361, 369–371.

Lee, D.H., Sherman, M.Y., Goldberg, A.L., 1996. Involvement of the molecular chaperone Ydj1 in the ubiquitin-dependent degradation of short-lived and abnormal proteins in *Saccharomyces cerevisiae*. Mol. Cell. Biol. 16, 4773–4781.

Meacham, G.C., Patterson, C., Zhang, W., Younger, J.M., Cyr, D.M., 2001. The Hsc70 co-chaperone CHIP targets immature CFTR for proteasomal degradation. Nat. Cell Biol. 3, 100–105.

Miyazaki, K., Fujita, T., Ozaki, T., Kato, C., Kurose, Y., Sakamoto, M., Kato, S., Goto, T., Itoyama, Y., Aoki, M., Nakagawara, A., 2004. NEDL1, a novel ubiquitin–protein isopeptide ligase for dishevelled-1, targets mutant superoxide dismutase-1. J. Biol. Chem. 279, 11327–11335.

Murata, S., Minami, Y., Minami, M., Chiba, T., Tanaka, K., 2001. CHIP is a chaperone-dependent E3 ligase that ubiquitylates unfolded protein. EMBO Rep. 2, 1133–1138.

Murata, S., Chiba, T., Tanaka, K., 2003. CHIP: a quality-control E3 ligase collaborating with molecular chaperones. Int. J. Biochem. Cell Biol. 35, 572–578.

Niwa, J., Ishigaki, S., Doyu, M., Suzuki, T., Tanaka, K., Sobue, G., 2001. A novel centrosomal ring-finger protein, dorfin, mediates ubiquitin ligase activity. Biochem. Biophys. Res. Commun. 281, 706–713.

Niwa, J., Ishigaki, S., Hishikawa, N., Yamamoto, M., Doyu, M., Murata, S., Tanaka, K., Taniguchi, N., Sobue, G., 2002. Dorfin ubiquitylates mutant SOD1 and prevents mutant SOD1-mediated neurotoxicity. J. Biol. Chem. 277, 36793–36798.

Oyake, D., Nishikawa, H., Koizuka, I., Fukuda, M., Ohta, T., 2002. Targeted substrate degradation by an engineered double RING ubiquitin ligase. Biochem. Biophys. Res. Commun. 295, 370–375.

Rosen, D.R., Siddique, T., Patterson, D., Figlewicz, D.A., Sapp, P., Hentati, A., Donaldson, D., Goto, J., O'Regan, J.P., Deng, H.X., et al., 1993. Mutations in Cu/Zn superoxide dismutase gene are associated with familial amyotrophic lateral sclerosis. Nature 362, 59–62.

Ross, C.A., Poirier, M.A., 2004. Protein aggregation and neurodegenerative disease. Nat. Med. 10, S10–S17 (Suppl.).

Rowland, L.P., Shneider, N.A., 2001. Amyotrophic lateral sclerosis. N. Engl. J. Med. 344, 1688–1700.

Sakamoto, K.M., Kim, K.B., Kumagai, A., Mercurio, F., Crews, C.M., Deshaies, R.J., 2001. Protacs: chimeric molecules that target proteins to the Skp1-Cullin-F box complex for ubiquitination and degradation. Proc. Natl. Acad. Sci. U. S. A. 98, 8554–8559.

Sakamoto, K.M., Kim, K.B., Verma, R., Ransick, A., Stein, B., Crews, C.M., Deshaies, R.J., 2003. Development of Protacs to target cancer-promoting proteins for ubiquitination and degradation. Mol. Cell Proteomics 2, 1350–1358.

Scheffner, M., Nuber, U., Huibregtse, J.M., 1995. Protein ubiquitination involving an E1–E2–E3 enzyme ubiquitin thioester cascade. Nature 373, 81–83.

Sherman, M.Y., Goldberg, A.L., 2001. Cellular defenses against unfolded proteins: a cell biologist thinks about neurodegenerative diseases. Neuron 29, 15–32.

Shimura, H., Schwartz, D., Gygi, S.P., Kosik, K.S., 2004. CHIP–Hsc70 complex ubiquitinates phosphorylated tau and enhances cell survival. J. Biol. Chem. 279, 4869–4876.

Tanaka, K., Suzuki, T., Hattori, N., Mizuno, Y., 2004. Ubiquitin, proteasome and parkin. Biochim. Biophys. Acta 1695, 235–247.

Urushitani, M., Kurisu, J., Tateno, M., Hatakeyama, S., Nakayama, K., Kato, S., Takahashi, R., 2004. CHIP promotes proteasomal degradation of familial ALS-linked mutant SOD1 by ubiquitinating Hsp/Hsc70. J. Neurochem. 90, 231–244.

Yoshida, Y., Tokunaga, F., Chiba, T., Iwai, K., Tanaka, K., Tai, T., 2003. Fbs2 is a new member of the E3 ubiquitin ligase family that recognizes sugar chains. J. Biol. Chem. 278, 43877–43884.

Neurobiology of Disease

Reversible Disruption of Dynactin 1-Mediated Retrograde Axonal Transport in Polyglutamine-Induced Motor Neuron Degeneration

Masahisa Katsuno, Hiroaki Adachi, Makoto Minamiyama, Masahiro Waza, Keisuke Tokui, Haruhiko Banno, Keisuke Suzuki, Yu Onoda, Fumiaki Tanaka, Manabu Doyu, and Gen Sobue

Department of Neurology, Nagoya University Graduate School of Medicine, Showa-ku, Nagoya 466-8550, Japan

Spinal and bulbar muscular atrophy (SBMA) is a hereditary neurodegenerative disease caused by an expansion of a trinucleotide CAG repeat encoding the polyglutamine tract in the *androgen receptor* (*AR*) gene. To elucidate the pathogenesis of polyglutamine-mediated motor neuron dysfunction, we investigated histopathological and biological alterations in a transgenic mouse model of SBMA carrying human pathogenic AR. In affected mice, neurofilaments and synaptophysin accumulated at the distal motor axon. A similar intramuscular accumulation of neurofilament was detected in the skeletal muscle of SBMA patients. Fluoro-gold labeling and sciatic nerve ligation demonstrated an impaired retrograde axonal transport in the transgenic mice. The mRNA level of dynactin 1, an axon motor for retrograde transport, was significantly reduced in the SBMA mice resulting from pathogenic AR-induced transcriptional dysregulation. These pathological events were observed before the onset of neurological symptoms, but were reversed by castration, which prevents nuclear accumulation of pathogenic AR. Overexpression of dynactin 1 mitigated neuronal toxicity of the pathogenic AR in a cell culture model of SBMA. These observations indicate that polyglutamine-dependent transcriptional dysregulation of dynactin 1 plays a crucial role in the reversible neuronal dysfunction in the early stage of SBMA.

Key words: polyglutamine; spinal and bulbar muscular atrophy; androgen; neurofilament; axonal transport; retrograde; dynactin

Introduction

Spinal and bulbar muscular atrophy (SBMA), or Kennedy's disease, is a hereditary neurodegenerative disease resulting from a loss of bulbar and spinal motor neurons (Kennedy et al., 1968; Sobue et al., 1989). Patients present with muscle atrophy and weakness of proximal limbs associated with bulbar palsy, tongue atrophy and contraction fasciculation (Katsuno et al., 2006). The disease affects exclusively adult males, whereas females carrying the mutant *androgen receptor* (*AR*) are seldom symptomatic (Schmidt et al., 2002). The molecular basis of SBMA is an expansion of a trinucleotide CAG repeat, which encodes the polyglutamine tract in the first exon of the *AR* gene (La Spada et al., 1991). This type of mutation has also been found to cause a variety of neurodegenerative disorders, termed polyglutamine diseases, such as Huntington's disease (HD), several forms of spinocerebellar ataxia, and dentatorubral pallidoluysian atrophy (Gatchel and Zoghbi, 2005). Although expression of the causative gene in each of these diseases is ubiquitous, selective neuronal cell death is observed in disease-specific areas of the CNS, suggesting a common molecular basis for these polyglutamine diseases.

Nuclear accumulation of pathogenic protein containing elongated polyglutamine is a crucial step in the pathophysiology of these diseases, providing an important therapeutic target (Adachi et al., 2005; Banno et al., 2006). The aberrant polyglutamine protein has a propensity to form aggregates in the nucleus and inhibits the function of transcriptional factors and coactivators, resulting in transcriptional perturbation (Cha, 2000; Gatchel and Zoghbi, 2005). In support of this hypothesis, altered expression of a variety of genes has been demonstrated in transgenic mouse models of polyglutamine diseases (Sugars and Rubinsztein, 2003). Although polyglutamine-induced transcriptional dysregulation is likely to be central to the pathogenesis of polyglutamine diseases, it has yet to be elucidated which genes are responsible for the selective neurodegeneration (Gatchel and Zoghbi, 2005).

No treatments have been established for polyglutamine diseases, but the androgen blockade therapy, surgical or medical castration, has shown striking therapeutic effects in the SBMA transgenic mouse model (Katsuno et al., 2002, 2003; Chevalier-Larsen et al., 2004). Androgen deprivation strongly inhibits the ligand-dependent nuclear accumulation of pathogenic AR protein, resulting in a striking improvement in neurological and histopathological findings of male mice.

In the present study, we investigated the molecular pathophysiology of motor neuron dysfunction in a transgenic mouse

Received July 18, 2006; revised Sept. 21, 2006; accepted Oct. 6, 2006.

This work was supported by a Center of Excellence grant from the Ministry of Education, Culture, Sports, Science and Technology, Japan, and by grants from the Ministry of Health, Labor and Welfare, Japan. We have no financial conflict of interest that might be construed to influence the results or interpretation of this manuscript. We thank Jun-ichi Miyazaki for kindly providing the pCAGGS vector.

Correspondence should be addressed to Dr. Gen Sobue, Department of Neurology, Nagoya University Graduate School of Medicine, 65 Tsurumai-cho, Showa-ku, Nagoya 466-8550, Japan. E-mail: sobueg@med.nagoya-u.ac.jp.

DOI:10.1523/JNEUROSCI.3032-06.2006

 0270-6474/06/2612106-12$15.00/0

model of SBMA. Polyglutamine-induced transcriptional dysregulation of the dynactin p150 subunit (dynactin 1), an axonal motor-associated protein, resulted in perturbation of retrograde axonal transport in spinal motor neurons in the early stage of the disease. These processes were reversed by castration, which inhibits nuclear accumulation of pathogenic AR. A defect in axonal trafficking of neurofilaments and synaptic vesicles, the potential molecular basis for the reversible pathogenesis, appears to contribute to the initiation of symptoms, and may account for the selective degeneration of motor neurons in SBMA.

Materials and Methods

Generation and maintenance of transgenic mouse. AR-24Q and AR-97Q mice were generated as described previously (Katsuno et al., 2002). Briefly, the full-length human *AR* fragment harboring 24 or 97 CAGs was subcloned into the *Hind*III site of the pCAGGS vector (Niwa et al., 1991) and microinjected into BDF1-fertilized eggs. Five founders with AR-97Q were obtained. These mouse lines were maintained by backcrossing them to C57BL/6J mice. All symptomatic lines (2–6, 4–6, and 7–8) were examined in the present study. All animal experiments were approved by the Animal Care Committee of the Nagoya University Graduate School of Medicine. Mice were given sterile water *ad libitum*. In the experiments where it was called for, sodium butyrate [a histone deacetylase (HDAC) inhibitor] was administered at a concentration of 4 g/L in distilled water from 5 weeks of age until the end of the analysis, as described previously (Minamiyama et al., 2004).

Neurological testing and castration after onset. Mice were subjected to the Rotarod task (Economex Rotarod; Colombus Instruments, Columbus, OH), and cage activity was measured (AB system; Neuroscience, Tokyo, Japan) as described previously (Katsuno et al., 2002). Gait stride was measured in 50 cm of footsteps, and the maximum value was recorded for each mouse. The onset of motor impairment was determined using weekly rotarod task analyses. Male AR-97Q mice were castrated or sham-operated via the abdominal route under ketamine–xylazine anesthesia (50 mg/kg ketamine and 10 mg/kg xylazine, i.p.) within 1 week after the onset of rotarod impairment.

Immunohistochemistry and immunofluorescent analysis. Ten-micrometer-thick sections were prepared from paraffin-embedded tissues, and immunohistochemistry was performed as described previously (Katsuno et al., 2002). Formalin-fixed tail samples were washed with 70% ethanol and decalcified with 7% formic acid–70% ethanol for 7 d before embedding in paraffin. Sections to be immunostained for dynactin 1, dynein intermediate chain, dynein heavy chain, and dynamitin were first microwaved for 20 min in 50 mM citrate buffer, pH 6.0. Sections to be immunostained for polyglutamine (1C2 antibody) were treated with formic acid for 5 min at room temperature. The following primary antibodies were used: anti-dynactin 1 (p150^{glued}, 1:250; BD Transduction, San Diego, CA), anti-dynein intermediate chain (1:500; Millipore, Temecula, CA), anti-dynein heavy chain (1:100; Sigma-Aldrich, St. Louis, MO), anti-dynamitin (1:1000; BD Transduction), anti-polyglutamine, 1C2 (1:10,000; Millipore), antiphosphorylated high molecular weight neurofilament (NF-H) (SMI31, 1:1000; Sternberger Monoclonals, Lutherville, MD), anti-nonphosphorylated NF-H (SMI32, 1:5000; Sternberger Monoclonals), and anti-synaptophysin (1:10,000; Dako, Glostrup, Denmark).

For immunofluorescent analysis of skeletal muscle, mice were deeply anesthetized with ketamine–xylazine and perfused with PBS followed by 4% paraformaldehyde fixative in phosphate buffer, pH 7.4. Gastrocnemius muscles were dissected free, frozen quickly by immersion in cooled acetone and powdered CO_2. Longitudinal, 30 μm, cryostat sections were placed on a silane-coated slide in a drop of 3% disodium EDTA, air dried at room temperature, and fixed in methanol/acetone (50:50 v/v). After blocking with PBS containing 5% goat serum and 1% BSA for 30 min at room temperature, sections were incubated with 5 μg/ml Oregon green-conjugated α-bungarotoxin (Invitrogen, Eugene, OR) for 60 min at room temperature. Sections were incubated with antiphosphorylated NF-H (SMI31, 1:5000; Sternberger Monoclonals), anti-synaptophysin (1:50,000; Dako), or anti-Rab3A (1:5000; BD Transduction) antibodies at 4°C overnight, and then with Alexa-546-conjugated goat anti-mouse IgG (1:1000; Invitrogen). Sections were examined with an IX71 inverted microscope (Olympus, Tokyo, Japan). For double staining of the skeletal muscle, paraffin-embedded sections were treated with TNB blocking buffer (PerkinElmer, Boston, MA) and incubated with anti-AR antibody (N-20, 1:500; Santa Cruz Biotechnology, Santa Cruz, CA) together with antiphospho-NF-H.

For immunostaining of human tissues, autopsy specimens of lumbar spinal cord and intercostal muscle obtained from a genetically diagnosed SBMA patient (78-year-old male) and those from a neurologically normal patient (75 years old) were used. The collection of tissues and their use for this study were approved by the Ethics Committee of Nagoya University Graduate School of Medicine. Spinal cord sections at 10 μm were incubated with anti-dynactin 1 antibody (p150^{glued}, 1:250; BD Transduction). Thirty-micrometer-thick cryostat sections of intercostal muscle were incubated with 150 μg/ml Alexa-488-conjugated α-bungarotoxin (Invitrogen) and then with antiphosphorylated NF-H (SMI31, 1:200; Sternberger Monoclonals).

Retrograde Fluoro-gold neurotracer labeling. For labeling neurons with intramuscular injection of tracer, mice were anesthetized with ketamine–xylazine, and a small incision was made in the skin of the left calf to expose the gastrocnemius muscle. A total volume of 4.5 μl of 2.5% Fluoro-gold solution (Biotium, Hayward, CA) in PBS was injected in three different parts of the muscle (proximal, middle, and distal) using a 10 μl Hamilton syringe. For labeling by the nerve stump method, the sciatic nerve was exposed and transected at mid-thigh level. A small polyethylene tube containing 2.5% Fluoro-gold solution was applied to the proximal stump of the cut sciatic nerve, and sealed with Vaseline to prevent leakage. Mice were anesthetized 44 h after Fluoro-gold administration with ketamine–xylazine and perfused with PBS followed by 4% paraformaldehyde in phosphate buffer, pH 7.4. Spinal cords were removed and postfixed with 4% paraformaldehyde in phosphate buffer for 2 h, floated in 10 and 15% sucrose for 4 h each and in 20% sucrose overnight. The samples were sectioned longitudinally on a cryostat at 30 μm and mounted on silane-coated slides. The number of Fluoro-gold labeled motor neurons was counted in serial spinal cord sections with an IX71 inverted microscope (Olympus) using a wide-band UV filter. Some specimens were immunostained for dynactin immediately after the number of Fluoro-gold-labeled motor neurons was counted.

Western blot analysis. SH-SY5Y cells were lysed in CellLytic lysis buffer (Sigma-Aldrich) containing a protease inhibitor mixture (Roche, Mannheim, Germany) 2 d after transfection. Mice were killed under ketamine–xylazine anesthesia. Their tissues were snap-frozen with powdered CO_2 in acetone and homogenized in 50 mM Tris, pH 8.0, 150 mM NaCl, 1% NP-40, 0.5% deoxycholate, 0.1% SDS, and 1 mM 2-mercaptoethanol containing 1 mM PMSF and 6 μg/ml aprotinine and then centrifuged at 2500 × *g* for 15 min at 4°C. The supernatant fractions were separated on 5–20% SDS-PAGE gels (10 μg protein for the nerve roots or 40 μg for the spinal cord, per lane) and then transferred to Hybond-P membranes (Amersham Pharmacia Biotech, Buckinghamshire, UK), using 25 mM Tris, 192 mM glycine, 0.1% SDS, and 10% methanol as transfer buffer. Immunoblotting was performed using the following primary antibodies: anti-dynactin 1 (p150^{glued}, 1:250; BD Transduction), anti-dynein intermediate chain (1:1000; Millipore), anti-dynein heavy chain (1:200; Sigma-Aldrich), anti-dynamitin (1:250; BD Transduction), anti-α-tubulin (1:5000; Sigma-Aldrich), antiphosphorylated NF-H (SMI31, 1:100,000; Sternberger Monoclonals), and anti-nonphosphorylated NF-H (SMI32, 1:1000; Sternberger Monoclonals). The immunoblots were digitalized (LAS-3000 imaging system; Fujifilm, Tokyo, Japan), signal intensities of three independent blots were quantified with Image Gauge software version 4.22 (Fujifilm), and the means ± SD were expressed in arbitrary units.

Ligation of mouse sciatic nerve. Under anesthesia with ketamine–xylazine, the skin of the right lower limb was incised. The right sciatic nerve was exposed and ligated at mid-thigh level using surgical thread. For immunofluorescent analysis, operated mice were decapitated under deep anesthesia with ketamine–xylazine 8 h after ligation and perfused with 4% paraformaldehyde fixative in phosphate buffer, pH 7.4. The right sciatic nerve segment, including at least 5 mm both proximal and distal to

the ligated site, was removed. The nonligated, left sciatic nerve was also taken out in the same manner as the right nerve. The removed nerves were placed into fixative for 4 h, transferred consecutively to 10, 15, and 20% sucrose in 0.01 M PBS, pH 7.4, for 4 h each at 4°C, mounted in Tissue-Tek OCT compound (Sakura, Tokyo, Japan), and frozen with powdered CO_2 in acetone. Ten-micrometer-thick cryostat sections were prepared from the frozen tissues, blocked with normal goat serum (1:20), incubated with anti-synaptophysin (1:50,000; Dako) at 4°C overnight, and then with Alexa-546-conjugated goat anti-mouse IgG (1:1000; Invitrogen). Immunofluorescent images were recorded with an IX71 inverted microscope (Olympus), and the signal intensities were quantified using Image Gauge software, version 4.22 (Fujifilm) and expressed in arbitrary units.

For immunoblotting of axonal proteins, the sciatic nerve segments 1 mm both proximal and distal to the ligated site were removed without paraformaldehyde fixation, and frozen in with powdered CO_2 in acetone. Protein extraction and Western blotting were performed as described above.

In situ *hybridization*. Formalin-fixed, paraffin-embedded 6-μm-thick sections of the spinal cord were deparaffinized, treated with proteinase K, and processed for *in situ* hybridization using an ISHR kit (Nippon Gene, Tokyo, Japan) according to the manufacturer's instructions. Dynactin 1 cDNA was obtained from spinal cords of wild-type mice. The primers, 5′-AGATGGTGGAGATGCTGACC-3′ and 5′-GAGCCTTGGTCTCAGCAAAC-3′, were phosphorylated with T4polynucleotide kinase (Stratagene Cloning Systems, La Jolla, CA). The cDNA was inserted into the pSPT 19 vector (Roche). Dioxigenin-labeled cRNA antisense and sense probes, 380 bp long, were generated from this plasmid using T7 and SP6 polymerase (Roche), respectively. Spinal cord sections were hybridized for 16 h at 42°C washed in formamide–4× SSC (50:50 v/v) at the same temperature, treated with RNase A at 37°C, and washed again in 0.1× SSC at 42°C. The signals were detected immunologically with alkaline phosphatase-conjugated anti-dioxigenin antibody and incubated with NBT/BCIP (Roche) for 16 h at 42°C. Slices were counterstained with methyl green. To quantify the intensity of the signals in the cell bodies of spinal motor neurons, three nonconsecutive sections from a wild-type littermate and those of a transgenic mouse from lines 7–8 or 4–6 were analyzed using the NIH Image program (version 1.62). Sections adjacent to those used for *in situ* hybridization were processed for immunohistochemistry using anti-polyglutamine antibody as described above.

Quantitative real-time PCR. Dynactin 1 mRNA levels were determined by real-time PCR as described before (Ishigaki et al., 2002; Ando et al., 2003). Briefly, total RNA (5 μg each) from AR-97Q and wild-type spinal cord were reverse transcribed into first-strand cDNA using SuperScript II reverse transcriptase (Invitrogen). Real-time PCR was performed in a total volume of 50 μl, containing 25 μl of 2× QuantiTect SYBR Green PCR Master Mix and 0.4 μM of each primer (Qiagen, Valencia, CA), and the product was detected by the iCycler system (Bio-Rad Laboratories, Hercules, CA). The reaction conditions were 95°C for 15 min and then 45 cycles of 15 s at 95°C followed by 60 s at 55°C. For an internal standard control, the expression level of glyceraldehyde-3-phosphate dehydrogenase (GAPDH) was simultaneously quantified. The following primers used were 5′-CTCAGAGGAGCCCAGATGA-3′ and 5′-GCTGGTCTTGCGGTACAGT-3′ for dynactin 1, 5′-GAGAGCATGGAGCTGGTGTA-3′ and 5′-CCAACCACGAAGTTGTTGAC-3′ for dynein intermediate chain, 5′-TACCAGGTGGGAGTGCATTA-3′ and 5′-CAGTCACTATGCCCATGACC-3′ for dynein heavy chain, 5′-ACAAGCGTGGAACACATCAT-3′ and 5′-TCTTTCCAATGCGATCTGAG-3′ for dynamitin, and 5′-CCTGGAGAAACCTGCCAAGTAT-3′ and 5′-TGAAGTCGCAGGAGACAACCT-3′ for GAPDH. The threshold cycle of each gene was determined as the number of PCR cycles at which the increase in reporter fluorescence was 10 times the baseline signal. The weight of the gene contained in each sample was equal to the log of the starting quantity and the standardized expression level in each mouse was equal to the weight ratio of each gene to that of GAPDH.

For the real-time PCR with mRNA extracted from SH-SY5Y cells, the following primers were used: 5′-CTTGGAAGCGATGAATGAGA-3′ and 5′-TAGTCTGCAACGTCTCCTG-3′ for dynactin 1, and 5′-AGCCTCAAGATCATCAGCAAT-3′ and 5′-GGACTGTGGTCATGAGTCCTT-3′ for GAPDH.

Plasmid vectors and cell culture. Human AR cDNAs containing 24 or 97 CAG repeats were subcloned into pcDNA3.1 (Invitrogen) as described previously (Kobayashi et al., 2000). Human dynactin 1 cDNA was also subcloned into pcDNA3.1 (Invitrogen). The human neuroblastoma cells (SH-SY5Y, #CRL-2266; American Type Culture Collection, Manassas, VA) were plated in 6-well dishes in 2 ml of DMEM/F12 containing 10% fetal bovine serum with penicillin and streptomycin, and each dish was transfected with 2 μg of the vector containing AR24, AR97, or mock and with 2 μg of the vector containing dynactin 1 or mock using Opti-MEM (Invitrogen) and Lipofectamine 2000 (Invitrogen) and then differentiated in differentiation medium (DMEM/F12 supplemented with 5% fetal calf serum and 10 μM retinoic acid) for 2 d. Two days after transfection, cells were stained with propidium iodide (Invitrogen, Eugene, OR) and mounted in Gelvatol. Quantitative analyses were made from triplicate determinations. Duplicate slides were graded blindly in two independent trials as described previously (Katsuno et al., 2005).

Statistical analyses. We analyzed data using the Kaplan-Meier and log-rank test for survival rate, ANOVA with *post hoc* test (Dunnett) for multiple comparisons, and an unpaired *t test* from Statview software version 5 (Hulinks, Tokyo, Japan).

Results

Accumulation of axonal proteins in distal motor axons of SBMA mouse

To clarify the molecular basis of neuronal dysfunction in SBMA, we analyzed histopathological alterations in the spinal cords of transgenic mice carrying full-length human *AR* with 97 CAGs (AR-97Q mice) (Katsuno et al., 2002, 2003). We first focused on the expression and phosphorylation level of NF-H because affected mice demonstrate axonal atrophy in the ventral nerve root (Katsuno et al., 2002). Although it has been widely accepted that NF-H phosphorylation is a crucial factor determining axon caliber, neither the amounts nor the phosphorylation levels of NF-H in spinal cord or ventral root were decreased in male AR-97Q mice compared with wild-type littermates (supplemental Fig. 1*A–C*, available at www.jneurosci.org as supplemental material). The distribution of NF-H in the anterior horn of AR-97Q mice was also indistinguishable from that of wild-type or AR-24Q mice bearing human AR with a normal polyglutamine length (Fig. 1*A*). However, AR-97Q mice demonstrated a striking accumulation of both phosphorylated and nonphosphorylated NF-H in skeletal muscle, a phenomenon not observed in AR-24Q or wild-types (Fig. 1*A*). Although motor neurons originating in the anterior horn are always affected in SBMA, because the primary motor neurons projecting their axons to the anterior horn are not affected, no accumulation is seen in this region. The damage to motor neurons originating within the anterior horn results in accumulation of NFs in the skeletal muscle, instead of the spinal cord. A similar accumulation of the middle molecular weight NF was also observed (data not shown). To clarify whether this phenomenon is specific to neurofilaments, we performed immunohistochemistry on both spinal cord and muscle with an antibody against synaptophysin, a transmembrane glycoprotein of synaptic vesicles that is also retrogradely transported in axons (Li et al., 1995). In AR-97Q mice, synaptophysin accumulated among the muscle fibers in a pattern similar to that of NF-H, whereas no such accumulation was observed in unaffected mice (Fig. 1*B*).

We then investigated the time course of abnormally accumulated NF in skeletal muscle. Because the onset of motor dysfunction occurs at 9–10 weeks in AR-97Q mice, NF pathology before and after the onset was examined. Anti-NF immunostaining demonstrated that intramuscular NF accumulation was detectable as early as 7 weeks before the onset of muscle weakness in this

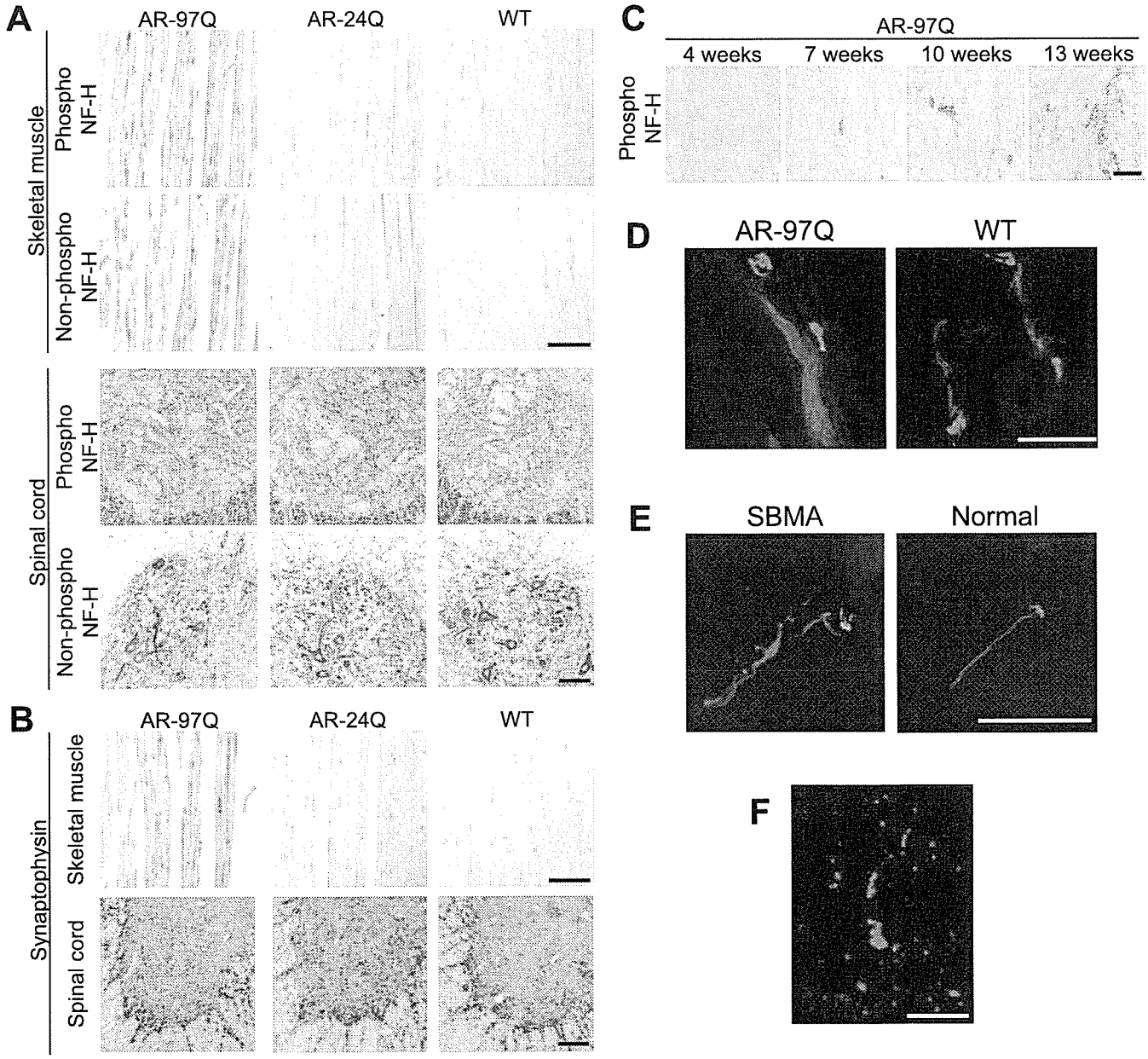

Figure 1. Accumulation of neurofilament and synaptophysin in the distal end of motor axons. ***A***, Immunohistochemistry of skeletal muscle and spinal cord from AR-97Q (4–6), AR-24Q, and wild-type mice (12 weeks) using an antibody for phosphorylated or nonphosphorylated NF-H. ***B***, Immunohistochemistry for synaptophysin shows findings parallel to those of neurofilament. ***C***, Age-dependent change in antiphosphorylated NF-H immunohistochemistry in skeletal muscle of SBMA mice. ***D***, Immunofluorescence of mouse skeletal muscle using α-bungarotoxin (green) in combination with antiphospho-NF-H antibody (red). Phosphorylated NF-H accumulates in the distal end of motor axons in AR-97 mice (7–8, 12 weeks). ***E***, Antiphospho-NF-H immunofluorescence with α-bungarotoxin staining in skeletal muscle from a human SBMA patient showing similar neurofilament accumulation. ***F***, Double-labeling of skeletal muscle from an AR-97Q mouse (4–6, 12 weeks) using antiphospho-NF-H antibody (green) and anti-AR (red) shows that accumulated NF-H does not colocalize with AR. Scale bars, 100 μm.

mouse model, and aggravated thereafter (Fig. 1*C*). These observations suggest that intramuscular accumulation of NF plays a role in the motor neuron dysfunction in this mouse model of SBMA.

To confirm the distribution of NF-H and synaptophysin in skeletal muscle, we examined the localization of these proteins in relation to the neuromuscular junction. Immunohistochemistry using α-bungarotoxin to mark the junctions, and fluorescent-labeled antibodies showed that both NF-H and synaptophysin accumulated in the most distal motor axon adjacent to neuromuscular junctions (Fig. 1*D*). A similar intramuscular accumulation of neurofilament was detected in the skeletal muscle of SBMA patients (Fig. 1*E*). Although pathogenic AR accumulated in the nuclei of skeletal muscle in the AR-97Q mice, the accumulation of NF-H did not colocalize with AR (Fig. 1*F*). Moreover, immunoprecipitation demonstrated no interaction between AR and NF-H (data not shown). These findings exclude the possibility that pathogenic AR directly interrupts the axonal trafficking.

Retrograde axonal transport is disrupted in SBMA mouse

To elucidate the molecular basis of the abnormal distribution of NF and synaptophysin, we studied axonal transport in this mouse model of SBMA. Axonal components undergo anterograde and/or retrograde axonal transport. Proteins including NF and synaptophysin are bidirectionally transported, whereas some

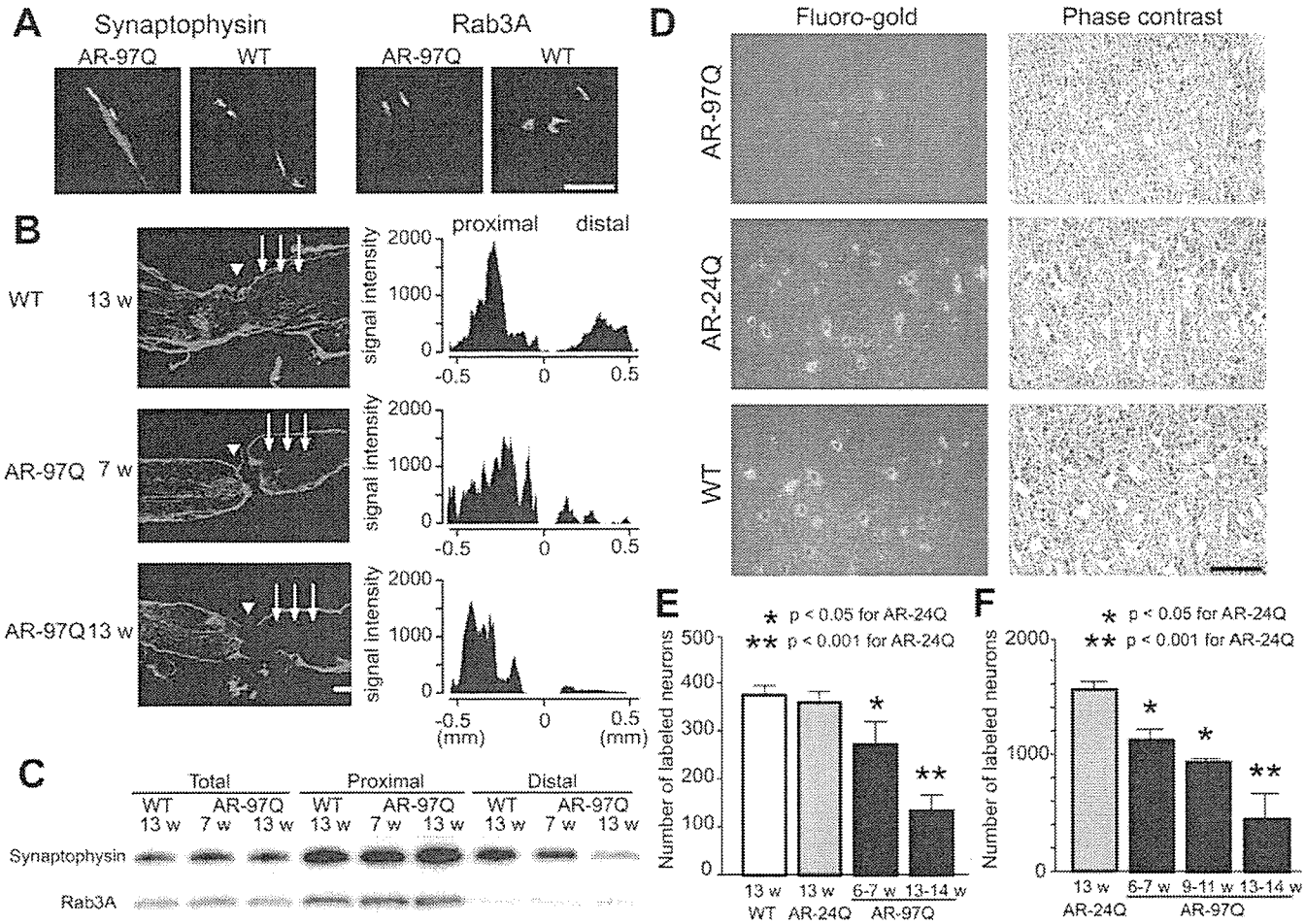

Figure 2. Perturbation of retrograde axonal transport in SBMA mice. ***A***, Immunofluorescence of mouse skeletal muscle using α-bungarotoxin (green) labeling the endplate together with anti-synaptophysin antibody (red) or anti-Rab3A antibody (red). Accumulation of Rab3A is not detected in wild-type or AR-97Q mice (7–8, 12 weeks). ***B***, Immunohistochemistry for synaptophysin in the sciatic nerve 8 h after ligation and representative quantification of immunoreactivity. Accumulation of synaptophysin immunoreactivity is decreased on the distal side (arrows) of the ligation site (arrowhead) in preonset (7 weeks) and advanced stage (13 weeks) AR-97Q mice. ***C***, Immunoblots of the sciatic nerve segments on both proximal and distal sides of the ligation. The total amount of proteins extracted from the contralateral nonligated sciatic nerve was analyzed as a control. ***D***, ***E***, Retrograde labeling of lumbar motor neurons of AR-97Q (7–8), AR-24Q, or wild-type mice (12 weeks) by Fluoro-gold injection into the gastrocnemius muscle (***D***) and the number of labeled neurons (***E***) ($n = 5$ for each group). ***F***, The number of motor neurons labeled by Fluoro-gold using the sciatic nerve stump method ($n = 5$ for each group). Scale bars: ***A***, ***B***, ***D***, 100 μm. Error bars indicate SD.

components such as Rab3A, a small GTP binding protein, are transported only anterogradely (Li et al., 1995; Roy et al., 2000). The distribution of Rab3A in skeletal muscle of SBMA mice was equivalent to that of wild-type mice, whereas synaptophysin and neurofilaments accumulated in the most distal motor axons of the SBMA mice only (Figs. 1*D*, 2*A*).

To further examine the nature of the axonal transport anomaly in SBMA mice, the sciatic nerve was ligated at mid-thigh level. Because the transport rate of NF is slower than other axonal components, we analyzed the transport of synaptophysin and Rab3A in this ligation study (Fig. 2*B*,*C*). In wild-type mice, synaptophysin accumulated predominantly on the proximal side of the ligation, but also on the distal side. Although synaptophysin and Rab3A accumulations proximal to the site of ligation were notable in both preonset and advanced stages of AR-97Q mice, their accumulation on the distal side was decreased before the onset of symptoms and was progressively inhibited. These findings suggest that disrupted retrograde axonal transport gives rise to the accumulation of axonal proteins in the distal motor axon terminals of SBMA mice before the onset of motor impairment.

To confirm this hypothesis, we analyzed retrograde neuronal labeling with the fluorescent tracer Fluoro-gold after its injection into the mouse calf muscle. The number of Fluoro-gold-labeled spinal motor neurons was significantly less in affected AR-97Q mice compared with AR-24Q or wild-type mice (Fig. 2*D*,*E*). To exclude the possibility that synaptic pathology contributed to diminished uptake of the tracer, we also examined Fluoro-gold labeling using direct application of the tracer into the sciatic nerve stump (Sagot et al., 1998). Again, AR-97Q mice showed fewer motor neurons labeled by Fluoro-gold applied directly to the proximal stump of the sciatic nerve than did the AR-24Q mice (Fig. 2*F*), suggesting that neither synaptic retraction nor disconnection is the basis for disruption of axonal transport. Furthermore, it should be noted that the decrease in the number of labeled neurons preceded the onset of motor symptoms in both of these experiments. These observations suggest that the disruption of retrograde transport plays an early role in the pathogenesis of motor neuron degeneration in SBMA.

Transcriptional dysregulation of dynactin 1 in SBMA

Retrograde axonal transport is microtubule-dependent and is regulated by the axon motor protein dynein and its associated protein complex, dynactin. To elucidate the molecular

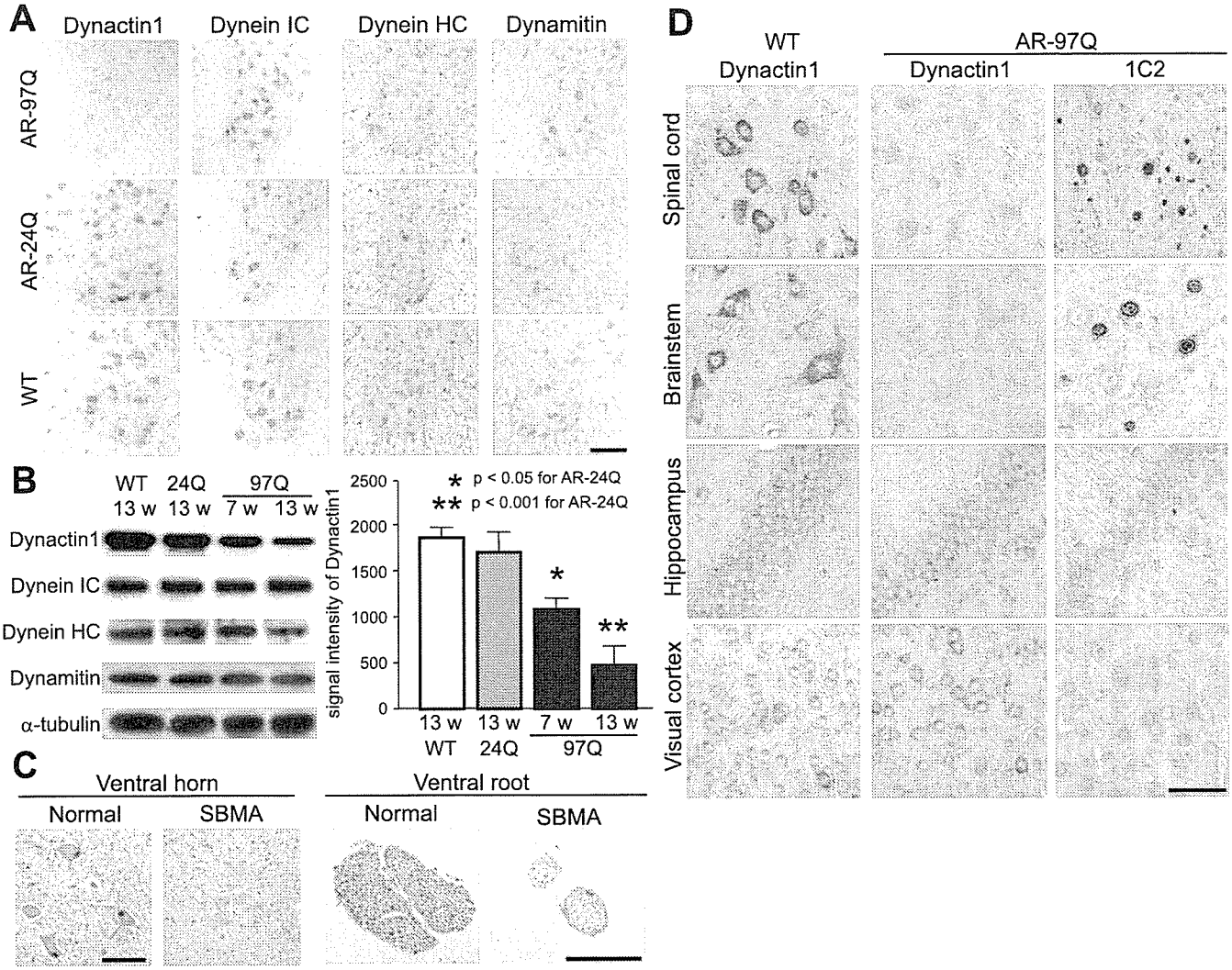

Figure 3. Decreased levels of dynactin 1 in SBMA. ***A***, Immunohistochemistry for motor proteins regulating retrograde axonal transport, dynactin 1, dynein intermediate chain (IC), dynein heavy chain (HC), and dynamitin in the spinal cord from AR-97Q (4–6), AR-24Q, and wild-type mice (12 weeks). Dynactin 1 is markedly diminished in the motor neurons of AR-97Q mice. ***B***, Western blot analysis for motor proteins in the ventral spinal root from presymptomatic or advanced AR-97Q mice (4–6) compared with those from AR-24Q and wild-type mice. ***C***, Dynactin 1 immunohistochemistry in the anterior horn and the ventral root of an SBMA patient and a normal subject. ***D***, Anti-dynactin 1 immunohistochemistry in various affected (spinal cord and brainstem) and nonaffected (hippocampus and visual cortex) tissues from wild-type and AR-97Q mice. Data from AR-97Q mice are compared with immunohistochemistry using the anti-polyglutamine antibody, 1C2. Scale bars: ***A***, 100 μm; ***C***, ***D***, 50 mm. Error bars indicate SD.

mechanism compromising retrograde axonal transport in SBMA mice, we examined the levels of various dynein and dynactin protein subunits. Immunohistochemistry of spinal cord sections demonstrated that the spinal motor neurons from AR-97Q mice had lower levels of dynactin 1, the largest subunit of dynactin, than did those from either wild-type or AR-24Q mice (Fig. 3*A*). In the ventral root, significantly decreased levels of dynactin 1 were apparent before the onset of motor symptoms (Fig. 3*B*). Although the level of dynein heavy chain was diminished in the advanced disease stage in SBMA mice, this phenomenon was not observed before the onset of symptoms (Fig. 3*B*). No alterations were observed in the levels of dynein intermediate chain or dynamitin, the p50 subunit of dynactin, throughout the disease course (Fig. 3*A*,*B*). To confirm the role of dynactin 1 in the pathogenesis of human SBMA, we also examined the protein level in autopsy specimens. As observed in the mouse model, the protein level of dynactin 1 was decreased in the anterior horn cells and in the ventral roots of SBMA patients (Fig. 3*C*).

To examine the cell specificity of reduced dynactin 1 levels we compared anti-dynactin 1 immunohistochemistry with that of anti-polyglutamine using the 1C2 antibody in various tissues from wild-type and AR-97Q mice (Fig, 3*D*). The immunoreactivity of dynactin 1 was markedly diminished in 1C2-positive tissues, but not in those lacking nuclear polyglutamine staining. This observation suggests that the reduction in dynactin 1 is relevant to the polyglutamine-mediated neuropathology. In addition, to investigate whether reduced levels of dynactin 1 were correlated with defective retrograde axonal transport, we analyzed anti-dynactin 1 immunohistochemistry in spinal cord sections labeled by Fluoro-gold (supplemental Fig. 2, available at www.jneurosci.org as supplemental material). The levels of dynactin 1 were decreased in the spinal motor neurons of AR-97Q mice concomitantly with decreased intensities of Fluoro-gold labeling. Together, these data strongly suggest that depletion of dynactin 1 is responsible for the disruption of retrograde axonal transport in SBMA.

To clarify the pathological mechanism responsible for reduc-

ing the levels of dynactin 1 protein in SBMA, mRNA levels were determined by *in situ* hybridization in AR-97Q and wild-type mice. Although dynactin 1 mRNA was expressed in virtually all motor neurons in the anterior horn, the expression was markedly repressed in AR-97Q mice (Fig. 4*A*). Moreover, the levels of dynactin 1 mRNA were significantly lower in those motor neurons demonstrating nuclear accumulation of pathogenic AR compared with those without 1C2 nuclear staining (Fig. 4*B*). Real-time quantitative PCR also demonstrated a significant decrease in dynactin 1 mRNA levels in the spinal cords of AR-97Q mice at all disease stages compared with those of wild-types (Fig. 4*C*). The level of dynein heavy chain mRNA was decreased in the advanced stage, but not in the preonset period. The levels of dynein intermediate chain mRNA and dynamitin mRNA were not altered either before or after the onset of motor symptoms.

To investigate the role that diminished levels of dynactin 1 play in neurodegeneration in SBMA, we tested whether overexpression of this protein suppressed the cellular toxicity usually observed in the presence of expanded polyglutamine. In SH-SY5Y cells bearing truncated AR containing an expanded polyglutamine, the level of dynactin 1 was decreased both in mRNA and in protein (Fig. 4*D*,*E*). In this cellular model of SBMA, overexpression of dynactin 1 alleviated cell death exerted by pathogenic AR (Fig. 4*E*).

In SBMA mice, the level of dynactin 1 protein in spinal motor neurons was restored by oral administration of sodium butyrate, an HDAC inhibitor that increases the level of histone acetylation leading to promotion of gene transcription (supplemental Fig. 3, available at www.jneurosci.org as supplemental material) (Minamiyama et al., 2004). Sodium butyrate-mediated upregulation of dynactin 1 also eventually alleviated the neurofilament accumulation in skeletal muscle (supplemental Fig. 3, available at www.jneurosci.org as supplemental material), although this treatment had no influence on the subcellular distribution of pathogenic AR protein (Minamiyama et al., 2004). These observations indicate that nuclear accumulation of aberrant AR in the nuclei of motor neurons leads to a decrease at the transcription level of dynactin 1, resulting in perturbation of retrograde axonal transport and subsequent motor neuron dysfunction.

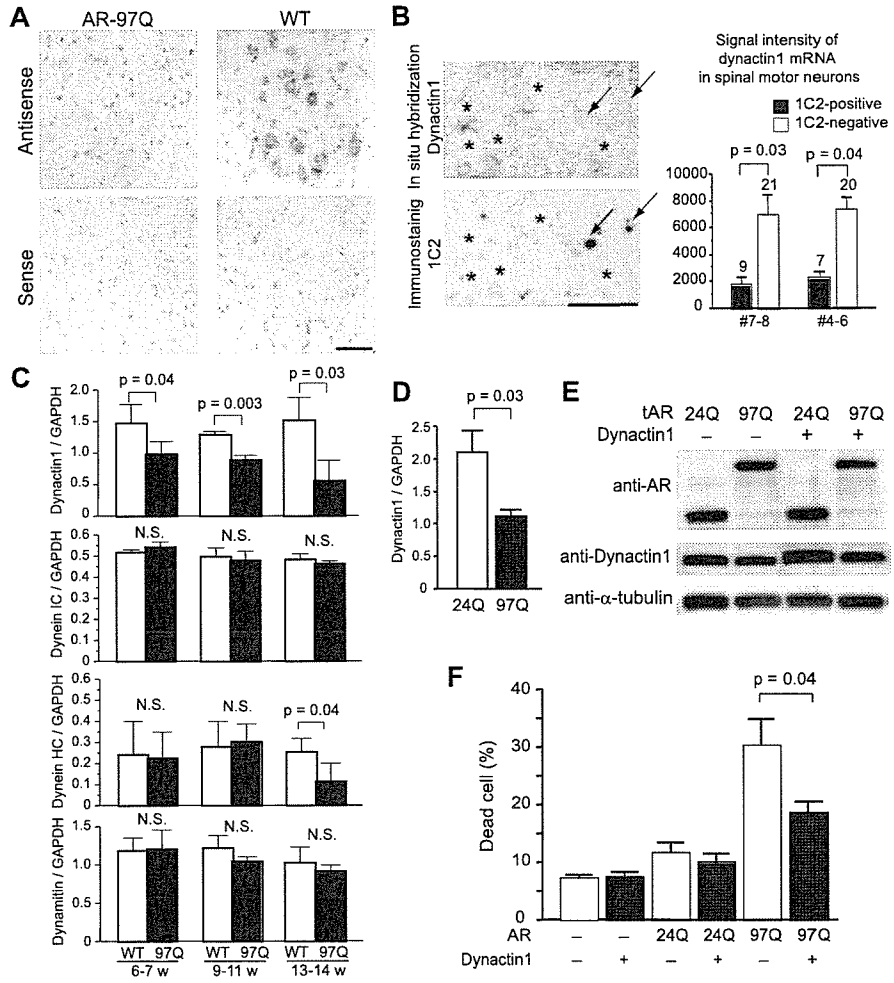

Figure 4. Transcriptional dysregulation of dynactin 1 in spinal motor neurons of SBMA mouse and effects of dynactin 1 overexpression. ***A***, *In situ* hybridization of dynactin 1 mRNA in the anterior horn of wild-type and AR-97 (4–6, 9 weeks) transgenic mice. Note the marked decrease in dynactin 1 mRNA levels in the spinal motor neurons of AR-97Q compared with those in wild-type mice. ***B***, *In situ* hybridization of dynactin 1 in the anterior horn. The adjacent sections were processed for anti-polyglutamine using the 1C2 antibody and the signals were quantified in representative AR-97Q mice (7–8, 9 weeks; 4–6, 10 weeks). Dynactin 1 mRNA expression is markedly decreased in the motor neurons demonstrating nuclear accumulation of pathogenic AR (arrows), but not in those lacking clear nuclear staining with anti-polyglutamine antibody (asterisks). The number above each bar indicates cell count. ***C***, The mRNA levels of dynactin 1 and other motor proteins in the spinal cords of wild-type and AR-97Q mice (7–8, 13 weeks) ($n = 4$ for each group) demonstrated by real-time, RT-PCR. Data shown are ratios of the various mRNA levels to GAPDH mRNA levels. ***D***, The mRNA levels of dynactin 1 in SH-SY5Y cells expressing either AR-24Q or AR-97Q ($n = 4$). ***E***, Immunoblots of SH-SY5Y cells expressing either AR-24Q or AR-97Q with or without overexpression of exogenous dynactin 1. ***F***, Frequency of cell death detected by propidium iodide staining. Dynactin 1 overexpression significantly reduced cell death in the cells bearing AR with elongated polyglutamine. Scale bars: ***A***, ***B***, 100 μm. Error bars indicate SD ($n = 6$ for each group). IC, Intermediate chain; HC, heavy chain.

Castration reverses symptoms and pathology of SBMA mouse

To examine the reversibility of the phenotypes resulting from polyglutamine-induced neuronal dysfunction, we investigated the effect of castration on early symptomatic SBMA mice. Male AR-97Q mice (7–8 and 4–6) demonstrate a rapid aggravation of neuromuscular phenotypes and usually succumb 3–4 weeks after the onset of motor impairment. The motor-impaired phenotype of the SBMA mouse is dependent on circulating testosterone levels, and we reported previously that castration during the presymptomatic period (4 weeks), to eliminate testosterone, drastically prevents the development of neurological symptoms such as weakness, amyotrophy, and shortened life span (Katsuno et al., 2002). In the present study, we castrated male AR-97Q mice within 1 week after the onset of rotarod task impairment. Castration reversed motor dysfunction in AR-97Q mice, even though it was performed after the onset of symptoms (Fig. 5*A*). Most mice showed a reduction in daily activity and body weight loss at the onset of rotarod task defect; these symptoms were also reversed by castration. In accordance with these observations,

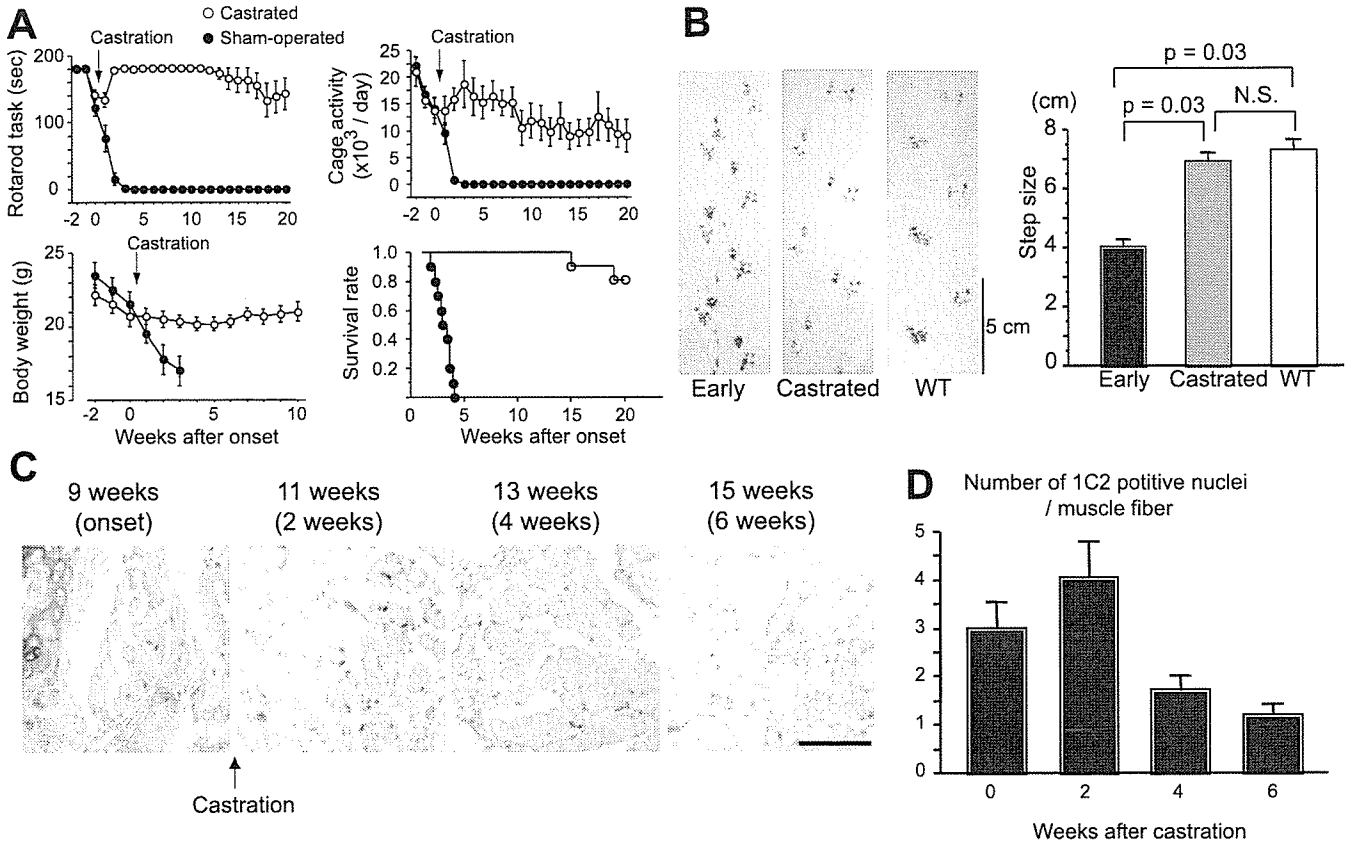

Figure 5. Symptomatic and histopathological reversibility of the SBMA phenotype in AR-97Q mice. ***A***, Castration of early symptomatic AR-97Q mice within 1 week after symptomatic manifestation resulted in significant improvement of the symptomatic phenotypes: rotarod task (7–8), cage activity (4–6), body weight (4–6), and survival rate (4–6). There are significant differences in all parameters between the sham-operated ($n = 10$) and castrated ($n = 10$) male AR-97Q mice ($p < 0.0001$, $p < 0.0001$, $p = 0.0001$, and $p = 0.0006$, respectively). ***B***, Representative footprints of an individual AR-97Q mouse (2–6) at the early onset of motor symptoms and after he had been castrated within 1 week after the onset of rotarod impairment, compared with those of a wild-type mouse. Quantification of the gait stride data ($n = 4$). ***C***, Nuclear accumulation of pathogenic AR with expanded polyglutamine in the tail muscle of one individual male AR-97Q mouse (4–6). ***D***, Castration after motor impairment onset significantly reduced the number of nuclei stained by an anti-polyglutamine antibody, 1C2 ($n = 4$). Scale bar: ***C***, 100 μm. Error bars indicate SD.

postonset castration significantly prolonged the life span of the male AR-97Q mice. We confirmed the reversal of motor symptoms by analyzing gait strides in a series of mouse footsteps (Fig. 5*B*).

To confirm the rescue effects of castration on histopathology, we investigated the nuclear accumulation of pathogenic AR in the skeletal muscle of tail sections sampled over time from the same mouse. Although the number of nuclei positively stained with 1C2 continued to increase for 2 weeks after the castration, at 4 weeks there was a significant decrease in expanded polyglutamine AR-positive nuclei (Fig. 5*C*,*D*). This time course corresponds approximately to the that of the symptomatic improvements, suggesting that nuclear accumulation of pathologic AR contributes to neuronal dysfunction and consequent symptomatic manifestation in SBMA mice.

Castration reverses dynactin 1 expression and restores retrograde axonal transport

It is important to determine whether disrupted retrograde axonal transport resulting from transcriptional dysregulation of dynactin 1, contributes to the reversible motor neuronal dysfunction in the early disease stage of SBMA mice. We therefore investigated axonal transport and the level of dynactin 1 expression in transgenic mice within 1 week after the onset of rotarod task impairment. In this early stage of the disease, the mice already demonstrated a reduction in the number of spinal motor neurons labeled by Fluoro-gold (Fig. 6*A*). Castration of symptomatic AR-97Q mice restored Fluoro-gold staining in the spinal motor neurons to a similar level as seen in wild-types (compare Figs. 2*D*, 6*A*). Castration after the onset of muscle weakness reduced the intramuscular accumulation of neurofilaments and synaptophysin in AR-97Q mice (Fig. 6*B*,*C*). Immunohistochemistry of spinal cord showed that postsymptomatic castration also eliminated nuclear accumulation of pathogenic AR as detected by the 1C2 antibody, and restored anti-dynactin 1 immunoreactivity in motor neurons (Fig. 6*D*). Immunoblotting demonstrated that the level of dynactin 1 protein, but not that of dynein heavy chain, was decreased in the ventral root of AR-97Q mice in the early symptomatic stage (Fig. 6*E*). Castration after the onset of motor impairment restored dynactin 1 to its normal levels in the ventral root, whereas it had no effect on dynactin 1 expression in wild-type mice (Fig. 6*E*). These observations indicate that the castration-mediated restoration of dynactin 1 expression improves retrograde axonal transport and contributes to the reversal of neuromuscular phenotypes in SBMA mice at an early stage of the disease process.

Discussion

Reversibility of neuronal dysfunction in SBMA

The fundamental pathological feature of polyglutamine diseases is the loss of neurons in selected regions of the CNS. Neuronal cell death, however, is often undetectable in mildly affected HD pa-

tients despite the presence of definite clinical features (Vonsattel et al., 1985). The early HD symptoms may thus result from functional alterations within neurons rather than cell death (Walker et al., 1984). In mouse models of polyglutamine diseases, it has been postulated that neuronal dysfunction, without cell loss, is sufficient to cause neurological symptoms (Mangiarini et al., 1996; Clark et al., 1997). These observations indicate that the pathogenesis of polyglutamine diseases is potentially reversible at an early stage. This hypothesis is supported by the observation that arrest of gene expression after the onset of symptoms reverses behavioral and neuropathological abnormalities in conditional mouse models of polyglutamine diseases (Yamamoto et al., 2000; Zu et al., 2004). The present study supports this hypothesis in that castration after the onset of motor deficit reverses behavioral and histopathological abnormalities by preventing nuclear accumulation of the pathogenic AR protein. These findings imply that cellular protective responses successfully abrogate the toxicity of polyglutamine-containing pathogenic protein, unless it perpetually accumulates in the nucleus.

Protein quality control systems, including molecular chaperones, the ubiquitin-proteasome system, and autophagy have been shown to reduce polyglutamine toxicity in various animal models of polyglutamine diseases (Adachi et al., 2003; Ravikumar et al., 2004; Katsuno et al., 2005; Waza et al., 2005). It is thus logical that inhibition of AR translocation into the nucleus restores the protein degradation machinery, such as ubiquitin-proteasome system, leading to the reduction in the amount of aggregates as well as the improvement of neuronal dysfunction in the SBMA mice (Waza et al., 2005).

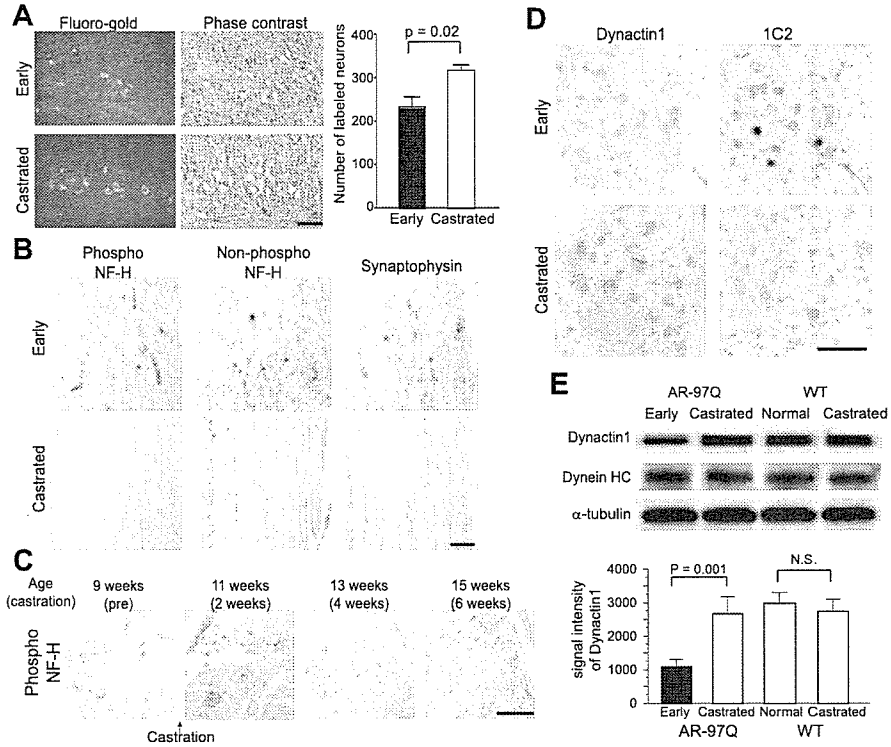

Figure 6. Hormonal intervention restores expression level of dynactin 1 and improves axonal transport. ***A***, Fluoro-gold labeling of spinal cord from early symptomatic (7–8; 9–11 weeks) and castrated (7–8; 13–16 weeks) male AR-97Q mice ($n = 5$ for each group). ***B***, Immunohistochemistry of skeletal muscle for NF-H and synaptophysin. ***C***, Immunohistochemistry for phosphorylated NF-H in the tail muscle of an individual male AR-97Q mouse (4–6). Castration after onset of symptoms depletes NF-H accumulation in the skeletal muscle. ***D***, Immunohistochemistry of the spinal cords of early symptomatic (4–6; 11 weeks) and castrated (4–6; 15 weeks) male AR-97Q mice using anti-dynactin 1 and 1C2. Castration eliminated nuclear accumulation of expanded polyglutamine AR. ***E***, Immunoblots of ventral roots from early symptomatic (4–6; 11 weeks) and castrated (4–6; 15 weeks) AR-97Q mice together with that from wild-type littermates (15 weeks) using antibodies against dynactin 1, dynein heavy chain (HC), and α-tubulin. Scale bars: ***A–D***, 100 μm. Error bars indicate SD ($n = 3$ for each group).

Defective retrograde axonal transport in SBMA

The SBMA mice we examined demonstrated impairment of retrograde axonal transport, resulting in the accumulation of neurofilaments and synaptophysin in the distal motor axon. Many proteins required for neuronal survival are synthesized within neuronal perikarya and are transported along the axon toward the synaptic terminals (Shea, 2000). A bidirectional delivery system consisting of anterograde and retrograde transport enables the recycling of cytoskeletons and synaptic vesicle-associated proteins. A histopathological hallmark of amyotrophic lateral sclerosis (ALS) is the accumulation of neurofilaments in cell bodies and proximal axons of affected motor neurons, presumably caused by compromised anterograde axonal transport; nevertheless, this finding has not been observed in SBMA (Sobue et al., 1990; Julien 2001). Transgenic SBMA mice demonstrate marked neurofilament storage in the distal motor axons, but not in the proximal axons or cell bodies. Neurofilament accumulation at motor endplates has also been reported in a transgenic mouse model of spinal muscular atrophy, another lower motor neuron disease (Cifuentes-Diaz et al., 2002). Axonal transport of NF depends on the dynein/dynactin system, disruption of which results in accumulation of neurofilaments at the distal axon in both cultured cells and transgenic mice (LaMonte et al., 2002; He et al., 2005). When combined, these findings indicate that the accumulation of axonal components in distal motor axons appears to be a substantial pathology associated with degeneration of lower motor neurons.

In the present study, synaptophysin showed an accumulation pattern similar to that of neurofilaments, whereas the distribution of Rab3A, another synaptic vesicle-associated protein, was not altered in this mouse model. Crush injury experiments have shown that although both proteins are delivered from cell bodies into axons, of the two only synaptophysin undergoes retrograde transport (Li et al., 1995, 2000). In addition, Fluoro-gold labeling experiments clearly demonstrated the disruption of retrograde, but not anterograde axonal transport in the spinal motor neurons of SBMA mice before the onset of muscle weakness. Together, the pathogenesis of motor neuronal dysfunction in SBMA is likely to be based on the perturbation of retrograde axonal transport, and not on an excessive transport of total axonal proteins.

Axonal transport impairment has been implicated in the pathogenesis of HD and SBMA (Gunawardena et al., 2003; Szebenyi et al., 2003). Although axonal inclusion interferes with axonal transport in a cell model of SBMA (Piccioni et al., 2002), AR containing expanded polyglutamine may also inhibit anterograde and/or retrograde axonal transport without visible aggregate formation (Szebenyi et al., 2003; Morfini et al., 2006). Accu-

mulation of neurofilaments at nerve terminals has also been documented in a mouse model of HD (Ribchester et al., 2004). In our SBMA mice, pathogenic AR did not colocalize with accumulated neurofilament, nor did it form axonal inclusions. More intriguingly, sodium butyrate-mediated gene upregulation attenuated the accumulation of neurofilaments, but did not alter the intracellular distribution of AR. These observations suggest that the defective retrograde axonal transport in SBMA mice does not result from the direct interaction between aberrant AR and axonal components, but rather from a secondary mechanism resulting from expanded polyglutamine.

Dynactin in motor neuron disease

The present study indicates that a decrease in the level of dynactin 1, the p150 subunit of dynactin, in affected neurons is a fundamental early event in the pathogenesis of SBMA. Dynactin is a multiprotein complex regulating dynein, a microtubule-dependent molecular motor for retrograde axonal transport. A mutation in *DCTN1*, the gene encoding dynactin 1, has been identified in a family with an autosomal dominant form of lower motor neuron disease and in another with ALS (Puls et al., 2003; Münch et al., 2005). A gene expression analysis of sporadic ALS patients revealed a significant decrease in dynactin 1 mRNA (Jiang et al., 2005). Overexpression of dynamitin dissociates the dynactin complex, resulting in late-onset motor neuron degeneration in a transgenic mouse model of motor neuron disease (LaMonte et al., 2002). These observations specifically link an impaired dynactin function to the pathogenesis of motor neuron diseases.

The pathological alteration in individual polyglutamine diseases is limited to distinct subsets of neurons, suggesting that the causative protein context influences the distribution of lesions. Motor neurons are selectively affected in SBMA, although pathogenic ARs are expressed in a wide range of neuronal and non-neuronal tissues (Doyu et al., 1994). A decreased level of dynactin 1 may contribute to this pathological selectivity, because a mutation in the *DCTN1* gene causes a lower motor neuron disease resembling SBMA (Puls et al., 2003, 2005).

Link between altered transcription and neuronal dysfunction

Numerous studies have shown that nuclear accumulation of pathogenic polyglutamine-proteins is essential for neurodegeneration, although cytoplasmic events may also contribute to the pathogenesis (Gatchel and Zoghbi, 2005). Polyglutamine aggregation sequesters a variety of fundamental cellular factors including heat shock proteins and proteasomal components as well as transcriptional factors and coactivators. cAMP response element-binding protein-binding protein (CBP), a transcriptional coactivator, colocalizes with intranuclear inclusions in SBMA patients as well as in transgenic SBMA mice (McCampbell et al., 2000; Nucifora et al., 2001). In addition to its sequestration in inclusion bodies, the histone acetyltransferase activity of CBP is also inhibited by soluble polyglutamine-protein (Steffan et al., 2001). This theory suggests that HDAC inhibitors, which upregulate transcription through acetylation of nuclear histone, may open new avenues in the development of therapeutics. In a fly model of HD, the HDAC inhibitors, sodium butyrate and suberoylanilide hydroxamic acid, increased histone acetylation, leading to the mitigation of neurodegeneration (Steffan et al., 2001). These compounds also improve motor dysfunction in mouse models of HD and SBMA (Hockly et al., 2003; Minamiyama et al., 2004).

In the present study, a reduction in the level of dynactin 1 protein is ascribed to polyglutamine-mediated transcriptional dysregulation, because the mRNA level of this protein is decreased in expanded polyglutamine AR-positive spinal motor neurons. It should be noted that this diminution was significant in the neurons demonstrating nuclear accumulation of pathogenic AR, implying that polyglutamine-induced transcriptional perturbation underlies this pathological process. This hypothesis is confirmed by the observation that administration of sodium butyrate, an HDAC inhibitor, restores dynactin 1 expression, resulting in elimination of neurofilament accumulation at distal motor axons. Although, because of the nonspecific nature of sodium butyrate, we cannot at this time rule out the possibility that expression of some other protein was also elevated, leading to the elimination of neurofilament accumulation.

Given that the expression of other axon motor proteins regulating retrograde axonal transport, such as dynein intermediate chain, dynein heavy chain and dynamitin are not altered before the onset of symptoms, the reduction in dynactin 1 appears to instigate the neurodegeneration in SBMA. In addition to our study, the selective perturbation of certain subsets of gene transcription has been demonstrated in other animal models of polyglutamine diseases (Sugars and Rubinsztein 2003; Sopher et al., 2004), although the precise mechanism has yet to be elucidated.

In summary, the present study demonstrates that the pathogenesis of SBMA is a reversible dysfunction of motor neurons that occurs in the early stages of the disease. Polyglutamine-induced transcriptional alteration of dynactin 1 appears to disrupt retrograde axonal transport, contributing to the early reversible neuronal dysfunction. These observations suggest that transcriptional alteration and subsequent involvement of retrograde axonal transport are substantial therapeutic targets for SBMA.

References

Adachi H, Katsuno M, Minamiyama M, Sang C, Pagoulatos G, Angelidis C, Kusakabe M, Yoshiki A, Kobayashi Y, Doyu M, Sobue G (2003) Heat shock protein 70 chaperone overexpression ameliorates phenotypes of the spinal and bulbar muscular atrophy transgenic mouse model by reducing nuclear-localized mutant androgen receptor protein. J Neurosci 23:2203–2211.

Adachi H, Katsuno M, Minamiyama M, Waza M, Sang C, Nakagomi Y, Kobayashi Y, Tanaka F, Doyu M, Inukai A, Yoshida M, Hashizume Y, Sobue G (2005) Widespread nuclear and cytoplasmic accumulation of mutant androgen receptor in SBMA patients. Brain 128:659–670.

Ando Y, Liang Y, Ishigaki S, Niwa J, Jiang Y, Kobayashi Y, Yamamoto M, Doyu M, Sobue G (2003) Caspase-1 and -3 mRNAs are differentially upregulated in motor neurons and glial cells in mutant SOD1 transgenic mouse spinal cord: a study using laser microdissection and real-time RT-PCR. Neurochem Res 28:839–846.

Banno H, Adachi H, Katsuno M, Suzuki K, Atsuta N, Watanabe H, Tanaka F, Doyu M, Sobue G (2006) Mutant androgen receptor accumulation in spinal and bulbar muscular atrophy scrotal skin: a pathogenic marker. Ann Neurol 59:520–526.

Cha JH (2000) Transcriptional dysregulation in Huntington's disease. Trends Neurosci 23:387–392.

Chevalier-Larsen ES, O'Brien CJ, Wang H, Jenkins SC, Holder L, Lieberman AP, Merry DE (2004) Castration restores function and neurofilament alterations of aged symptomatic males in a transgenic mouse model of spinal and bulbar muscular atrophy. J Neurosci 24:4778–4786.

Cifuentes-Diaz C, Nicole S, Velasco ME, Borra-Cebrian C, Panozzo C, Frugier T, Millet G, Roblot N, Joshi V, Melki J (2002) Neurofilament accumulation at the motor endplate and lack of axonal sprouting in a spinal muscular atrophy mouse model. Hum Mol Genet 11:1439–1447.

Clark HB, Burright EN, Yunis WS, Larson S, Wilcox C, Hartman B, Matilla A, Zoghbi HY, Orr HT (1997) Purkinje cell expression of a mutant allele of

SCA1 in transgenic mice leads to disparate effects on motor behaviors, followed by a progressive cerebellar dysfunction and histological alterations. J Neurosci 17:7385–7395.

Doyu M, Sobue G, Kimata K, Yamamoto K, Mitsuma T (1994) Androgen receptor mRNA with increased size of tandem CAG repeat is widely expressed in the neural and nonneural tissues of X-linked recessive bulbospinal neuronopathy. J Neurol Sci 127:43–47.

Gatchel JR, Zoghbi HY (2005) Diseases of unstable repeat expansion: mechanism and principles. Nat Rev Genet 6:743–755.

Gunawardena S, Her LS, Brusch RG, Laymon RA, Niesman IR, Gordesky-Gold B, Sintasath L, Bonini NM, Goldstein LS (2003) Disruption of axonal transport by loss of huntingtin or expression of pathogenic polyglutamine proteins in *Drosophila*. Neuron 40:25–40.

He Y, Francis F, Myers KA, Yu W, Black MM, Baas PW (2005) Role of cytoplasmic dynein in the axonal transport of microtubules and neurofilaments. J Cell Biol 168:697–703.

Hockly E, Richon VM, Woodman B, Smith DL, Zhou X, Rosa E, Sathasivam K, Ghazi-Noori S, Mahal A, Lowden PA, Steffan JS, Marsh JL, Thompson LM, Lewis CM, Marks PA, Bates GP (2003) Suberoylanilide hydroxamic acid, a histone deacetylase inhibitor, ameliorates motor deficits in a mouse model of Huntington's disease. Proc Natl Acad Sci USA 100:2041–2046.

Ishigaki S, Liang Y, Yamamoto M, Niwa J, Ando Y, Yoshihara T, Takeuchi H, Doyu M, Sobue G (2002) X-linked inhibitor of apoptosis protein is involved in mutant SOD1-mediated neuronal degeneration. J Neurochem 82:576–584.

Jiang YM, Yamamoto M, Kobayashi Y, Yoshihara T, Liang Y, Terao S, Takeuchi H, Ishigaki S, Katsuno M, Adachi H, Niwa J, Tanaka F, Doyu M, Yoshida M, Hashizume Y, Sobue G (2005) Gene expression profile of spinal motor neurons in sporadic amyotrophic lateral sclerosis. Ann Neurol 57:236–251.

Julien JP (2001) Amyotrophic lateral sclerosis: unfolding the toxicity of the misfolded. Cell 104:581–591.

Katsuno M, Adachi H, Kume A, Li M, Nakagomi Y, Niwa H, Sang C, Kobayashi Y, Doyu M, Sobue G (2002) Testosterone reduction prevents phenotypic expression in a transgenic mouse model of spinal and bulbar muscular atrophy. Neuron 35:843–854.

Katsuno M, Adachi H, Doyu M, Minamiyama M, Sang C, Kobayashi Y, Inukai A, Sobue G (2003) Leuprorelin rescues polyglutamine-dependent phenotypes in a transgenic mouse model of spinal and bulbar muscular atrophy. Nat Med 9:768–773.

Katsuno M, Sang C, Adachi H, Minamiyama M, Waza M, Tanaka F, Doyu M, Sobue G (2005) Pharmacological induction of heat-shock proteins alleviates polyglutamine-mediated motor neuron disease. Proc Natl Acad Sci USA 102:16801–16806.

Katsuno M, Adachi H, Waza M, Banno H, Suzuki K, Tanaka F, Doyu M, Sobue G (2006) Pathogenesis, animal models and therapeutics in spinal and bulbar muscular atrophy (SBMA). Exp Neurol 200:8–18.

Kennedy WR, Alter M, Sung JH (1968) Progressive proximal spinal and bulbar muscular atrophy of late onset. A sex-linked recessive trait. Neurology 18:671–680.

Kobayashi Y, Kume A, Li M, Doyu M, Hata M, Ohtsuka K, Sobue G (2000) Chaperones Hsp70 and Hsp40 suppress aggregate formation and apoptosis in cultured neuronal cells expressing truncated androgen receptor protein with expanded polyglutamine tract. J Biol Chem 275:8772–8778.

LaMonte BH, Wallace KE, Holloway BA, Shelly SS, Ascano J, Tokito M, Van Winkle T, Howland DS, Holzbaur EL (2002) Disruption of dynein/dynactin inhibits axonal transport in motor neurons causing late-onset progressive degeneration. Neuron 34:715–727.

La Spada AR, Wilson EM, Lubahn DB, Harding AE, Fischbeck KH (1991) Androgen receptor gene mutations in X-linked spinal and bulbar muscular atrophy. Nature 352:77–79.

Li JY, Jahn R, Dahlstrom A (1995) Rab3a, a small GTP-binding protein, undergoes fast anterograde transport but not retrograde transport in neurons. Eur J Cell Biol 67:297–307.

Li JY, Pfister KK, Brady ST, Dahlstrom A (2000) Cytoplasmic dynein conversion at a crush injury in rat peripheral axons. J Neurosci Res 61:151–161.

Mangiarini L, Sathasivam K, Seller M, Cozens B, Harper A, Hetherington C, Lawton M, Trottier Y, Lehrach H, Davies SW, Bates GP (1996) Exon 1 of the HD gene with an expanded CAG repeat is sufficient to cause a progressive neurological phenotype in transgenic mice. Cell 87:493–506.

McCampbell A, Taylor JP, Taye AA, Robitschek J, Li M, Walcott J, Merry D, Chai Y, Paulson H, Sobue G, Fischbeck KH (2000) CREB-binding protein sequestration by expanded polyglutamine. Hum Mol Genet 9:2197–2202.

Minamiyama M, Katsuno M, Adachi H, Waza M, Sang C, Kobayashi Y, Tanaka F, Doyu M, Inukai A, Sobue G (2004) Sodium butyrate ameliorates phenotypic expression in a transgenic mouse model of spinal and bulbar muscular atrophy. Hum Mol Genet 13:1183–1192.

Morfini G, Pigino G, Szebenyi G, You Y, Pollema S, Brady ST (2006) JNK mediates pathogenic effects of polyglutamine-expanded androgen receptor on fast axonal transport. Nat Neurosci 9:907–916.

Münch C, Rosenbohm A, Sperfeld AD, Uttner I, Reske S, Krause BJ, Sedlmeier R, Meyer T, Hanemann CO, Stumm G, Ludolph AC (2005) Heterozygous R1101K mutation of the DCTN1 gene in a family with ALS and FTD. Ann Neurol 58:777–780.

Niwa H, Yamamura K, Miyazaki J (1991) Efficient selection for high-expression transfectants with a novel eukaryotic vector. Gene 108:193–199.

Nucifora Jr FC, Sasaki M, Peters MF, Huang H, Cooper JK, Yamada M, Takahashi H, Tsuji S, Troncoso J, Dawson VL, Dawson TM, Ross CA (2001) Interference by huntingtin and atrophin-1 with cbp-mediated transcription leading to cellular toxicity. Science 291:2423–2428.

Piccioni F, Pinton P, Simeoni S, Pozzi P, Fascio U, Vismara G, Martini L, Rizzuto R, Poletti A (2002) Androgen receptor with elongated polyglutamine tract forms aggregates that alter axonal trafficking and mitochondrial distribution in motor neuronal processes. FASEB J 16:1418–1420.

Puls I, Jonnakuty C, LaMonte BH, Holzbaur EL, Tokito M, Mann E, Floeter MK, Bidus K, Drayna D, Oh SJ, Brown Jr RH, Ludlow CL, Fischbeck KH (2003) Mutant dynactin in motor neuron disease. Nat Genet 33:455–456.

Puls I, Oh SJ, Sumner CJ, Wallace KE, Floeter MK, Mann EA, Kennedy WR, Wendelschafer-Crabb G, Vortmeyer A, Powers R, Finnegan K, Holzbaur EL, Fischbeck KH, Ludlow CL (2005) Distal spinal and bulbar muscular atrophy caused by dynactin mutation. Ann Neurol 57:687–694.

Ravikumar B, Vacher C, Berger Z, Davies JE, Luo S, Oroz LG, Scaravilli F, Easton DF, Duden R, O'Kane CJ, Rubinsztein DC (2004) Inhibition of mTOR induces autophagy and reduces toxicity of polyglutamine expansions in fly and mouse models of Huntington disease. Nat Genet 36:585–595.

Ribchester RR, Thomson D, Wood NI, Hinks T, Gillingwater TH, Wishart TM, Court FA, Morton AJ (2004) Progressive abnormalities in skeletal muscle and neuromuscular junctions of transgenic mice expressing the Huntington's disease mutation. Eur J Neurosci 20:3092–3114.

Roy S, Coffee P, Smith G, Liem RK, Brady ST, Black MM (2000) Neurofilaments are transported rapidly but intermittently in axons: implications for slow axonal transport. J Neurosci 20:6849–6861.

Sagot Y, Rosse T, Vejsada R, Perrelet D, Kato AC (1998) Differential effects of neurotrophic factors on motoneuron retrograde labeling in a murine model of motoneuron disease. J Neurosci 18:1132–1141.

Schmidt BJ, Greenberg CR, Allingham-Hawkins DJ, Spriggs EL (2002) Expression of X-linked bulbospinal muscular atrophy (Kennedy disease) in two homozygous women. Neurology 59:770–772.

Shea TB (2000) Microtubule motors, phosphorylation and axonal transport of neurofilaments. J Neurocytol 29:873–887.

Sobue G, Hashizume Y, Mukai E, Hirayama M, Mitsuma T, Takahashi A (1989) X-linked recessive bulbospinal neuronopathy. A clinicopathological study. Brain 112:209–232.

Sobue G, Hashizume Y, Yasuda T, Mukai E, Kumagai T, Mitsuma T, Trojanowski JQ (1990) Phosphorylated high molecular weight neurofilament protein in lower motor neurons in amyotrophic lateral sclerosis and other neurodegenerative diseases involving ventral horn cells. Acta Neuropathol (Berl) 79:402–408.

Sopher BL, Thomas Jr PS, LaFevre-Bernt MA, Holm IE, Wilke SA, Ware CB, Jin LW, Libby RT, Ellerby LM, La Spada AR (2004) Androgen receptor YAC transgenic mice recapitulate SBMA motor neuronopathy and implicate VEGF164 in the motor neuron degeneration. Neuron 41:687–699.

Steffan JS, Bodai L, Pallos J, Poelman M, McCampbell A, Apostol BL, Kazant-

sev A, Schmidt E, Zhu YZ, Greenwald M, Kurokawa R, Housman DE, Jackson GR, Marsh JL, Thompson LM (2001) Histone deacetylase inhibitors arrest polyglutamine-dependent neurodegeneration in *Drosophila*. Nature 413:739–743.

Sugars KL, Rubinsztein DC (2003) Transcriptional abnormalities in Huntington disease. Trends Genet 19:233–238.

Szebenyi G, Morfini GA, Babcock A, Gould M, Selkoe K, Stenoien DL, Young M, Faber PW, MacDonald ME, McPhaul MJ, Brady ST (2003) Neuropathogenic forms of huntingtin and androgen receptor inhibit fast axonal transport. Neuron 40:41–52.

Vonsattel JP, Myers RH, Stevens TJ, Ferrante RJ, Bird ED, Richardson Jr EP (1985) Neuropathological classification of Huntington's disease. J Neuropathol Exp Neurol 44:559–577.

Walker FO, Young AB, Penney JB, Dovorini-Zis K, Shoulson I (1984) Benzodiazepine and GABA receptors in early Huntington's disease. Neurology 34:1237–1240.

Waza M, Adachi H, Katsuno M, Minamiyama M, Sang C, Tanaka F, Inukai A, Doyu M, Sobue G (2005) 17-AAG, an Hsp90 inhibitor, ameliorates polyglutamine-mediated motor neuron degeneration. Nat Med 11:1088–1095.

Yamamoto A, Lucas JJ, Hen R (2000) Reversal of neuropathology and motor dysfunction in a conditional model of Huntington's disease. Cell 101:57–66.

Zu T, Duvick LA, Kaytor MD, Berlinger MS, Zoghbi HY, Clark HB, Orr HT (2004) Recovery from polyglutamine-induced neurodegeneration in conditional SCA1 transgenic mice. J Neurosci 24:8853–8861.

THE JOURNAL OF BIOLOGICAL CHEMISTRY VOL. 281, NO. 17, pp. 11610–11617, April 28, 2006

Calcium-sensing Receptor Ubiquitination and Degradation Mediated by the E3 Ubiquitin Ligase Dorfin*

Received for publication, December 21, 2005, and in revised form, February 28, 2006 Published, JBC Papers in Press, March 2, 2006, DOI 10.1074/jbc.M513552200

Ying Huang[‡§], **Jun-ichi Niwa**[¶], **Gen Sobue**[¶], **and Gerda E. Breitwieser**[§1]

From the [‡]*Department of Biology, Syracuse University, Syracuse, New York 13244, the* [§]*Department of Neurology, Nagoya University Graduate School of Medicine, Nagoya 466-8500, Japan, and the* [¶]*Weis Center for Research, Geisinger Clinic, Danville, Pennsylvania 17822*

Calcium-sensing receptors (CaR) contribute to regulation of systemic calcium homeostasis by activation of G_q- and G_i-linked signaling pathways in the parathyroids, kidney, and intestine. Little is known about the mechanisms regulating CaR synthesis and degradation. Screening of a human kidney yeast two-hybrid library identified the E3 ubiquitin ligase dorfin as a binding partner for the intracellular carboxyl terminus of CaR. Interaction between CaR and dorfin was confirmed by coimmunoprecipitation from HEK293 cells. Ubiquitination of CaR was observed in the presence of the proteasomal inhibitor MG132; mutation of all putative intracellular loop and carboxyl-terminal lysine residues abolished ubiquitination of CaR. Coexpression with dorfin decreased the amount of total CaR protein and increased CaR ubiquitination, whereas a dominant negative fragment of dorfin had opposite effects. The AAA-ATPase p97/valosin-containing protein associates with both CaR and dorfin in HEK293 cells. Treatment with tunicamycin, an inhibitor of *N*-linked glycosylation, induced the appearance of the unglycosylated 115-kDa CaR form, which was further increased by exposure to MG132, or upon transfection with a dorfin dominant negative construct, suggesting that dorfin-mediated proteasomal degradation of immature CaR occurs from the endoplasmic reticulum. Because endogenous CaR in Madin-Darby canine kidney cells is also subject to degradation from the endoplasmic reticulum, dorfin-mediated ubiquitination may contribute to a general mechanism for CaR quality control during biosynthesis.

The calcium-sensing receptor (CaR)[2] contributes to maintenance of systemic Ca^{2+} homeostasis, regulating parathyroid hormone secretion and absorption/resorption of Ca^{2+} by the intestine and kidney and may also have effects on bone (1). CaR belongs to family C of the GPCR superfamily, having structural similarities to metabotropic glutamate receptors, γ-aminobutyric acid, type B receptors, and some putative pheromone/taste receptors (1, 2). Common to all members of family C is a large extracellular domain of more than 600 amino acids containing the agonist binding site, a heptahelical transmembrane domain, and a large intracellular carboxyl-terminal tail of more than 200 amino acids (1, 2). Members of Family C, including CaR, function as dimers, stabilized either by a disulfide bond or non-covalent interactions (3–5). The CaR extracellular domain contains *N*-linked glycosylation sites (2, 6, 7) and is stabilized by multiple intramolecular disulfide bonds, as well as one intermolecular disulfide bond between monomers in the dimer (8–10). Upon agonist stimulation, CaR activates diverse signaling pathways leading to changes in hormone secretion, cell proliferation, differentiation, and/or apoptosis (1). Although considerable progress has been made in understanding the structure, activation, and signaling of CaR, the biosynthesis, trafficking, targeting, and turnover mechanisms regulating CaR remain largely unexplored.

To identify novel proteins that might regulate trafficking and/or targeting of CaR, the intracellular carboxyl terminus of CaR was used as bait in a yeast two-hybrid (Y2H) screen of a human kidney cDNA library. One of the proteins identified in the screen was the E3 ubiquitin ligase dorfin (double-RING finger protein) (11). Dorfin was originally cloned from human spinal cord and is expressed in many organs, including kidney, liver, intestine, and the central nervous system (11). Dorfin localizes to a region near the centrosome in an aggresome-like structure in cultured cells (11). In the nervous system, dorfin ubiquitinates superoxide dismutase-1 (12) and synphilin-1 (13) and is a component of Lewy bodies observed in Parkinson's and other neurodegenerative diseases (12–14). Ubiquitination results in the attachment of ubiquitin, a highly conserved 76-amino acid polypeptide, to the ε-amino group of lysine residues of target proteins, and requires the sequential actions of three enzymes. Final transfer of activated ubiquitin to target proteins is coordinated by the E3 ligase, which specifically interacts with both E2-ubiquitin and the target protein (15). Dorfin contains two RING domains at its amino terminus, which function as recruiting motifs for specific E2s (11). The carboxyl terminus of dorfin has no identifiable motifs but has been shown to confer specificity of binding to synphilin-1 (13). Dorfin interacts directly with VCP (valosin-containing protein, also called p97 or Cdc48 homologue) (14), an AAA-ATPase proposed to have a role in endoplasmic reticulum-associated protein degradation (ERAD). VCP assists in translocation of ubiquitinated proteins from the ER and acts as a chaperone, targeting ubiquitinated proteins to the proteasome for degradation (16–19).

In this report, we characterize the functional interactions between CaR and dorfin in HEK293 cells and demonstrate that dorfin mediates CaR ubiquitination, leading to degradation by the proteasome. Both dorfin and CaR interact with VCP in HEK293 cells, and a dominant negative fragment of dorfin protects immature forms of CaR from degradation. Finally, endogenous CaR in MDCK cells is also subject to ER-associated degradation, suggesting a common mechanism may regulate quality control of both exogenously and endogenously expressed

* This work was supported by National Institutes of Health Grant GM58578 and funds from the Weis Center for Research (to G. E. B.), and the graduate program of the Department of Biology, Syracuse University (to Y. H.). The costs of publication of this article were defrayed in part by the payment of page charges. This article must therefore be hereby marked "*advertisement*" in accordance with 18 U.S.C. Section 1734 solely to indicate this fact.

[1] To whom correspondence should be addressed: Weis Center for Research, Geisinger Clinic, 100 N. Academy Ave., Danville, PA 17822-2604. Tel.: 570-271-6675; Fax: 570-271-5886; E-mail: gebreitwieser@geisinger.edu.

[2] The abbreviations used are: CaR, calcium-sensing receptor; CT, carboxyl terminus; DCT, dorfin carboxyl-terminal dominant negative fragment; ER, endoplasmic reticulum; ERAD, endoplasmic reticulum-associated degradation; GPCR, G protein-coupled receptor; VCP, valosin-containing protein; HEK293, human embryonic kidney 293; MDCK, Madin-Darby canine kidney; EGFP, enhanced green fluorescence protein; PBS, phosphate-buffered saline; RING, really interesting new gene; Y2H assay, yeast two-hybrid assay; X-α-gal, 5-bromo-4-chloro-3-indolyl-α-D-galactopyranoside; HA, hemagglutinin; ERK, extracellular signal-regulated kinase; E3, ubiquitin-protein isopeptide ligase.

CaR. These results suggest that dorfin may recognize misfolded or nonfunctional CaR at the endoplasmic reticulum, leading to ubiquitination and proteasomal degradation.

EXPERIMENTAL PROCEDURES

Materials—Human kidney cDNA library and all the materials for the Y2H screen were purchased from Clontech. HEK293 and MDCK cells were from the American Tissue Culture Collection and used through laboratory passage number 30. Restriction enzymes were from New England Biolabs and Promega. The EGFP-dorfin plasmid (dorfin chimera with EGFP at the amino terminus) and rabbit polyclonal antibody against dorfin (D-30) were generated as described previously (11). The HA-ubiquitin plasmid was generously provided by Dr. Richard J. H. Wojcikiewicz (SUNY Upstate Medical University, Syracuse, NY). Monoclonal antibodies were from various sources (anti-FLAG M2 and anti-actin antibodies, Sigma; anti-HA antibody, Roche Diagnostics; anti-VCP antibody, Research Diagnostics; and anti-GFP antibody, Molecular Probes). Rabbit polyclonal antibody against CaR (LRG) was generated as described (20). Anti-phospho-ERK1/2 (p42/44) polyclonal antibody was from Cell Signaling Technology. ECL anti-mouse and anti-rabbit, horseradish peroxidase-conjugated secondary antibodies were purchased from Amersham Biosciences. MG132 and tunicamycin were purchased from Sigma.

Plasmid Construction—CaR with an amino-terminal FLAG epitope (FLAG-CaR) was generated as described (21). CaR carboxyl-terminal (CaR-CT) fragments in the Y2H bait vector pGBKT7 were prepared by PCR using primers containing NdeI and SalI sites, using FLAG-CaR as template. PCR products were digested with NdeI/SalI and subcloned into NdeI/SalI-digested pGBKT7. Dorfin carboxyl-terminal fragments in the Y2H prey vector pACT2 were prepared similarly, using NcoI and XhoI sites. The dominant negative construct of dorfin was generated as a chimera with EGFP at the carboxyl terminus (DCT-EGFP). The DCT fragment containing dorfin residues 561–838 was prepared by PCR using primers containing BglII and SalI sites. The PCR product was digested with BglII/SalI and subcloned into BglII/SalI-digested PEGFP-N1 vector (Clontech). Another version of dominant negative dorfin (DCT-c-*myc*) was prepared similarly by PCR the DCT fragment using primers containing XbaI and HindIII sites. The PCR product was digested with XbaI/HindIII and subcloned into XbaI/HindIII-digested pcDNA3.1A(−) vector (Clontech). Another construct of dorfin (DNT-EGFP) containing the N-terminal RING-finger domains of dorfin from residue 1–367 was prepared by PCR using primers containing SacI and KpnI sites. The PCR product was digested with SacI/KpnI and subcloned into SacI/KpnI-digested pEGFP-N1 vector (Clontech). Point mutations were generated by a modified inverse PCR mutagenesis method (22). All PCR reactions used *Pfu* DNA polymerase (Stratagene). All constructs were verified by dideoxy-DNA sequencing (DNA Sequencing Facility, Cornell University, Ithaca, NY). Sequences of primers will be provided upon request.

Y2H Assay Screening—Gal4-based Y2H library screening was performed by yeast mating as recommended in the manufacturer's instructions (Clontech). Yeast *Saccharomyces cerevisiae* MATa strain AH109 was transformed with bait plasmid containing CaR-CT (amino acids 866–1078) and incubated with yeast *S. cerevisiae* MATα strain Y187 pretransformed with human kidney cDNA library (Clontech) in 2xYPDA/Kan at 30 °C for 24 h. The mixture was plated on SD/-Ade/-His/-Leu/-Trp plates to screen for $ADE2^+$ and $HIS3^+$ clones. Plates were incubated at 30 °C until colonies appeared. Colonies were restreaked on SD/-Ade/-His/-Leu/-Trp plus X-α-gal plates to screen for $MEL1^+$ clones. Clones that activated three reporter genes, *ADE2*, *HIS3*, and *MEL1*, were considered positive and identified by purifying plasmids and sequencing inserts.

Directed Y2H studies were performed by cotransformation using the lithium acetate method (23). Bait plasmids containing CaR-CT fragments and prey plasmids containing dorfin carboxyl-terminal fragments were cotransformed into AH109 and plated on SD/-Ade/-His/-Leu/-Trp plus X-α-gal plates. An interaction was considered positive when three reporter genes (ADE2, HIS3, and MEL1) were activated.

Cell Culture and Transfection—HEK293 and MDCK cells were grown in high glucose Dulbecco's modified Eagle's medium, supplemented with 10% heat-inactivated fetal calf serum, 50 units/ml penicillin, and 50 μg/ml streptomycin (37 °C, 5% CO_2). HEK293 cells were transiently transfected with Novafector (Venn Nova LLC, Pompano, FL) according to the manufacturer's instructions; experiments were done 72 h after transfection. For inhibitor studies, cells were treated with MG132 and/or tunicamycin (solubilized in Me_2SO) for 12 h prior to lysis. Comparable levels of Me_2SO had no effect on measured parameters.

SDS-PAGE and Western Blotting—Transfected HEK293 cells or MDCK cells were washed with PBS-EDTA and lysed on ice with PBS containing 5 mM EDTA, 0.5% Triton X-100, 10 mM iodoacetamide, plus protease inhibitor mixture (Roche Applied Science). Cell lysates were agitated for 30 min at 4 °C and cleared by centrifugation. Supernatants were mixed with loading buffer (12 M urea, 4% SDS, 0.01% bromphenol blue, 100 mM β-mercaptoethanol in 200 mM Tris) and separated on 4–15% SDS-polyacrylamide gels (Bio-Rad) before transfer to nitrocellulose membranes (Bio-Rad). Membranes were incubated with primary antibodies (GFP, 1:500; LRG, 1:1000; HA, 1:1000; actin, 1:1000; D-30, 1:3000; or VCP, 1:1000) overnight at 4 °C. Membranes were incubated with secondary antibody coupled to horseradish peroxidase (1:5000) at room temperature for 1 h. Proteins were visualized by enhanced chemiluminescence (Super West Pico Chemiluminescent Substrate, Pierce). Assay of ERK1/2 phosphorylation was as previously described (21). When the same blot was probed for the presence of coprecipitated proteins, nitrocellulose membranes were stripped in Restore Western blot Stripping Buffer (Pierce) and probed with a second primary antibody.

Immunoprecipitation—Transfected HEK293 cells were washed with PBS and lysed as described. After sonication on ice, samples were agitated for 30 min at 4 °C and incubated with 10 μl of protein G-agarose (Invitrogen) to minimize nonspecific binding. Samples were centrifuged, and supernatants were incubated with antibody for 3 h at 4 °C. 15 μl of protein G-agarose was then added, and samples were rotated overnight (4 °C). Precipitates were incubated in loading buffer for 30 min at 25 °C and run on SDS-polyacrylamide gels as described. To detect specific ubiquitination, a two-step immunoprecipitation was performed. After the first immunoprecipitation as described, pellets were washed three times with lysis buffer and incubated with 1% SDS/PBS for 30 min (25 °C) to disrupt non-covalent interactions. Samples were centrifuged, and supernatants were diluted with lysis buffer, followed by a second immunoprecipitation. The resultant precipitates were incubated in loading buffer and separated on SDS-polyacrylamide gels as described.

Densitometry and Statistics—Blots were digitized using an Epson Expression 800 Photo scanner and quantified by densitometry using AlphaEaseFC StandAlone Software (San Leandro, CA). Results were mean ± S.D. of at least three independent experiments; graphs were generated using Sigma Plot 2000. Student's *t* test (two comparisons) was performed, and $p < 0.05$ was considered significant.

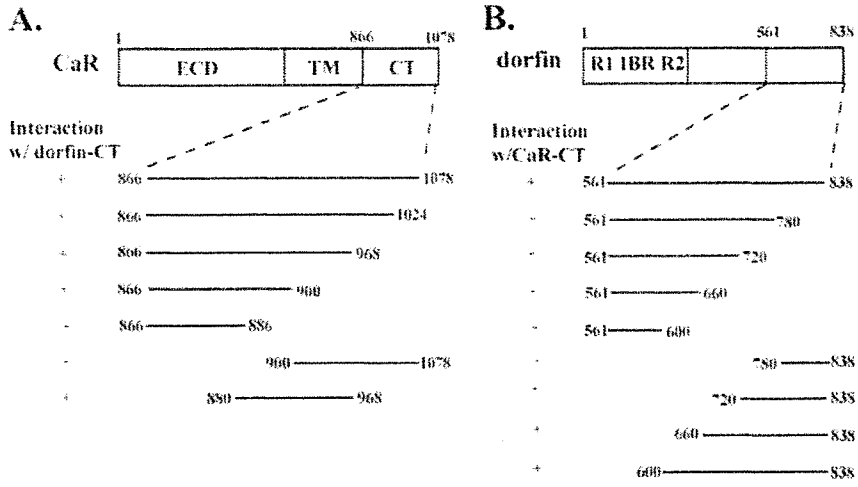

FIGURE 1. **Analysis of interaction sites on calcium-sensing receptor (CaR) and the E3 ubiquitin ligase dorfin by directed Y2H assay.** *A*, schematic representation of CaR and localization of the interaction site for dorfin carboxyl-terminal fragment (residues 561–838). The cytoplasmic carboxyl terminus of CaR (residues 866–1078) was truncated from both the amino and carboxyl termini as indicated and screened by cotransformation of the AH109 yeast strain with the CaR fragment plus the carboxyl terminus of dorfin (residues 561–838). *TM*, transmembrane heptahelical domain; *ECD*, extracellular domain. *B*, schematic representation of dorfin and localization of the interaction site for CaR carboxyl-terminal fragment (residues 866–1078). Truncations were generated from both the amino- and carboxyl-terminal ends of the dorfin fragment (residues 561–838) and screened by cotransformation of the AH109 yeast strain with the dorfin fragment plus the carboxyl terminus of CaR (residues 866–1078). *R1*, *R2*, RING finger domains; *IBR*, in between RING-finger domain. For *A* and *B*, positive interactions, resulting in activation of three reporter genes (*HIS3*, *ADE2*, and *MEL1*) are indicated as "+."

RESULTS

Y2H Screen Identifies the E3 Ubiquitin Ligase Dorfin as a CaR-binding Protein—The cytoplasmic carboxyl terminus of CaR (CT, residues 866–1078) was used as bait to screen a human kidney cDNA library (Fig. 1*A*). Positive clones were selected by activation of three reporter genes, *ADE2*, *HIS3*, and *MEL1*. Blast searches of the NCBI data base with positive clones identified in the screen yielded a fragment corresponding to the carboxyl terminus (residues 561–838) of the E3 ubiquitin ligase dorfin, an 838-amino acid protein (Fig. 1*B*) (11).

To localize the dorfin interaction site on the CaR carboxyl terminus, various truncations of the CaR carboxyl terminus (in pGBKT7), illustrated in Fig. 1*A*, were screened against the carboxyl terminus of dorfin (residues 561–838, in pACT2) after cotransformation in the AH109 strain. The full CaR-CT (residues 866–1078) interacted with dorfin, confirming the results of the initial screen. Truncations of the carboxyl end of CaR-CT were well tolerated, displaying positive interactions with dorfin. Only the smallest fragment, containing residues 866–886, did not interact with dorfin. Truncations from the amino terminus of the CaR-CT narrowed the region for interaction with dorfin to residues 880–900 (Fig. 1*A*).

Complementary directed Y2H screens were performed to localize the CaR-CT interaction site on the carboxyl terminus of dorfin (residues 561–838). Any truncations from the carboxyl terminus of dorfin inhibited interactions with CaR-CT, whereas interaction with CaR-CT was retained upon removal of up to 100 residues from the amino terminus of the dorfin fragment (residues 561–660). The minimal fragment of the dorfin carboxyl terminus required for interaction with CaR-CT contains residues from 660–838 (Fig. 1*B*).

Coimmunoprecipitation of CaR and Dorfin from HEK293 Cells Confirms Their Interaction—Human CaR having an amino-terminal FLAG epitope (FLAG-CaR) was transfected into HEK293 cells, and FLAG-CaR was immunoprecipitated with anti-FLAG antibody. The immunoprecipitate was separated on a 4–15% SDS-PAGE reducing gel, blotted to nitrocellulose, and probed with anti-dorfin antibody D-30. Endogenous dorfin was observed as a doublet with molecular mass of ~100 kDa in the presence (*lane 1*) but not in the absence (*lane 2*) of transfected FLAG-CaR (Fig. 2*A*, *top panel*). The two *lower panels* in Fig. 2 illustrate

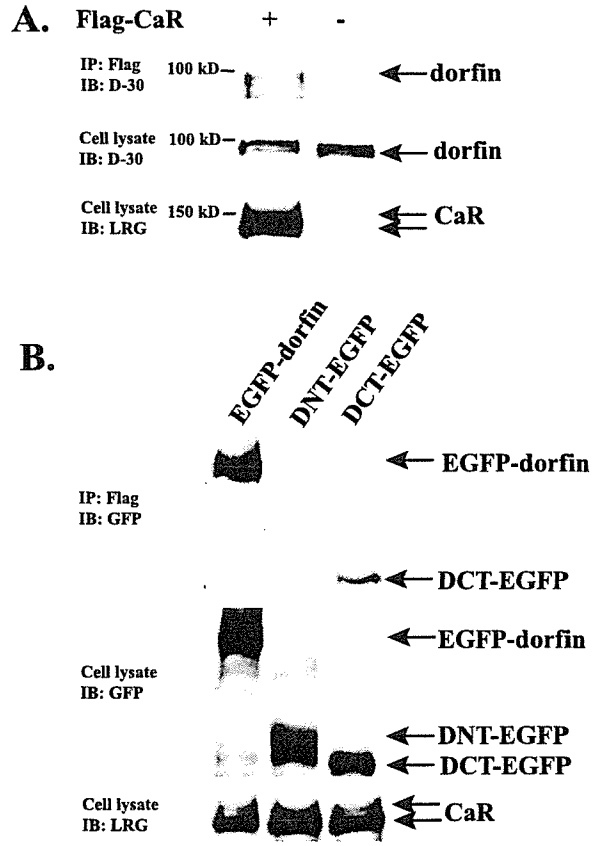

FIGURE 2. **Interaction of full-length CaR and dorfin in HEK293 cells.** *A*, HEK293 cells were transfected with (*lane 1*) or without (*lane 2*) FLAG-CaR cDNA. Cells were harvested 72 h after transfection. Anti-FLAG antibody was used to immunoprecipitate (*IP*) samples, and blots were probed with anti-dorfin antibody D-30 (*top panel*). Lysates were probed with anti-dorfin D-30 antibody (*middle panel*) or anti-CaR LRG antibody (*bottom panel*) to assess protein expression. *B*, FLAG-CaR cDNA-transfected HEK293 cells were cotransfected with EGFP-dorfin (*lane 1*), DNT-EGFP (*lane 2*), or DCT-EGFP (*lane 3*), respectively. Anti-FLAG antibody was used to immunoprecipitate samples, and blots were probed with anti-GFP antibody (*top panel*). Lysates were probed with anti-GFP antibody (*middle panel*) or anti-CaR LRG antibody (*lower panel*) to assess protein expression. *IB*, immunoblot.

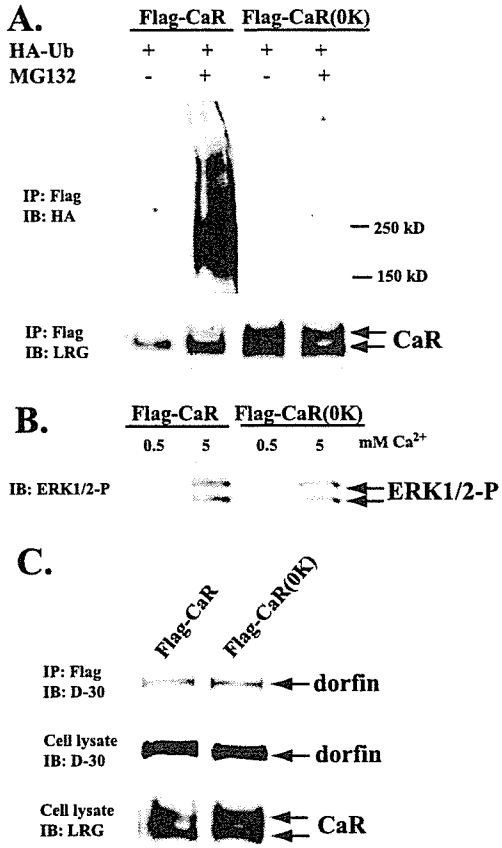

FIGURE 3. **Ubiquitination of CaR in HEK293 cells.** *A*, FLAG-CaR or FLAG-CaR(0K) cDNA was transfected into HEK293 cells with HA-Ub cDNA. Cells were incubated without (*lanes 1* and *3*) or with (*lanes 2* and *4*) 10 μM proteasomal inhibitor MG132 for 12 h prior to lysis. Cell lysates were immunoprecipitated (*IP*) with anti-FLAG antibody, and the precipitated pellets were treated with 1% SDS/PBS to disrupt non-covalent interactions. Supernatants were diluted with lysis buffer, followed by a second immunoprecipitation using anti-FLAG antibody. The blot was probed with anti-HA antibody (*upper panel*). The same blot was then stripped and probed with anti-CaR antibody LRG (*lower panel*). *B*, FLAG-CaR cDNA or FLAG-CaR(0K) cDNA was transfected into HEK293 cells. Cells were preincubated with 0.5 mM Ca^{2+} overnight prior to exposure to either 0.5 or 5 mM Ca^{2+} for 10 min (37 °C), followed by immunoblotting (*IB*) of lysates with anti-phospho-ERK1/2 antibody. *C*, FLAG-CaR cDNA or FLAG-CaR(0K) cDNA was transfected into HEK293 cells. Anti-FLAG antibody was used to immunoprecipitate samples, and blots were probed with anti-dorfin D-30 antibody (*top blot*). Lysates were probed with anti-dorfin D-30 antibody (*middle blot*) or anti-CaR LRG antibody (*bottom blot*).

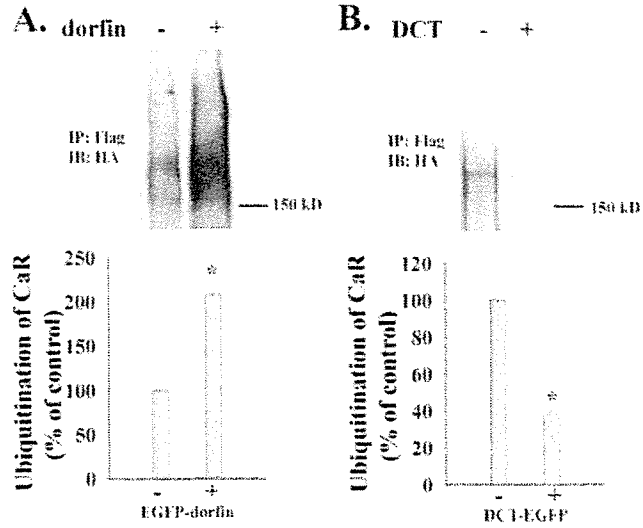

FIGURE 4. **Regulation of CaR ubiquitination by dorfin.** *A*, dorfin mediates ubiquitination of CaR. FLAG-CaR (3 μg) and HA-Ub (2 μg) cDNAs were cotransfected into HEK293 cells, without (−) or with (+) EGFP-dorfin cDNA (6 μg). Cells were incubated with 10 μM MG132 for 12 h prior to lysis. Cell lysates were immunoprecipitated (*IP*) with anti-FLAG antibody, and blots were probed with anti-HA antibody. CaR ubiquitination was quantified and normalized to basal ubiquitination in the absence of exogenous dorfin; significance at $p < 0.05$ (*). *B*, dominant negative dorfin fragment DCT inhibits ubiquitination of CaR. FLAG-CaR cDNA (3 μg) and HA-ubiquitin cDNA (2 μg) were cotransfected into HEK293 cells, without (−) or with (+) DCT-EGFP cDNA (6 μg). Methods were as described in *A*. *IB*, immunoblot.

the expression of endogenous dorfin (probed with anti-dorfin antibody D-30) or FLAG-CaR (probed with anti-CaR LRG antibody) in cell lysates. These results confirm the interaction of full-length CaR and dorfin in HEK293 cells.

To confirm that the dorfin fragment identified in the Y2H studies is required for the interaction of dorfin and CaR in mammalian cells, FLAG-CaR and full-length dorfin (EGFP-dorfin) or dorfin truncations (DNT-EGFP or DCT-EGFP) were tested for coimmunoprecipitation from HEK293 cells. DNT-EGFP contains the amino-terminal RING-finger domains of dorfin from residues 1–367; DCT-EGFP contains the carboxyl-terminal domain of dorfin from residues 561–838. Anti-FLAG antibody was used to immunoprecipitate FLAG-CaR, and blots were probed with anti-GFP antibody to detect the dorfin species. EGFP-dorfin (130 kDa) and DCT-EGFP (60 kDa) coprecipitated with FLAG-CaR (Fig. 2*B*, *top panel*), but DNT-EGFP (68 kDa) did not. The *middle* and *bottom panels* of Fig. 2*B* illustrate expression of the indicated constructs in cell lysates when probed with anti-GFP (*middle*) or anti-CaR LRG (*bottom*) antibodies. These results confirm that the domain of dorfin mediating the interaction with CaR in yeast, *i.e.* the carboxyl terminus, is also required for the interaction of dorfin with CaR in mammalian cells.

CaR Is Ubiquitinated—Interaction between CaR and dorfin suggests that CaR may be ubiquitinated. To test this possibility, FLAG-CaR and amino-terminal HA-tagged ubiquitin (HA-Ub) were cotransfected into HEK293 cells, and a two-step, denaturing protocol was used to immunoprecipitate FLAG-CaR. Briefly, anti-FLAG antibody was used to immunoprecipitate CaR, followed by treatment of the pellet with 1% SDS/PBS to disrupt non-covalent interactions between CaR and its associated proteins. The supernatant was diluted with lysis buffer and subjected to a second round of immunoprecipitation with anti-FLAG antibody. The Western blot was probed with anti-HA antibody to detect ubiquitinated species. Ubiquitination of CaR was observed in the presence of the proteasomal inhibitor MG132, appearing in the range from 150 to >250 kDa, while ubiquitination was barely detectable in the absence of MG132 (Fig. 3*A*, *upper panel, lanes 1* and *2*). MG132 increased the amount of CaR protein (Fig. 3*A*, *lower panel, lanes 1* and *2*), suggesting that ubiquitination followed by proteasomal degradation contributes to regulation of CaR.

Ubiquitin ligases covalently conjugate ubiquitin to lysine residues of target proteins. To confirm that CaR is ubiquitinated, we mutated intracellular lysine residues to arginine. There are nine lysine residues within the CaR carboxyl terminus (residues 863, 882, 897, 917, 931, 963, 965, 984, and 1002) and seven lysine residues within the three intracellular loops (residues 636, 644, 709, 717, 793, 796, and 805). When each lysine residue was mutated to arginine individually, the resulting mutants were still heavily ubiquitinated (data not shown). Because single point mutations did not abolish ubiquitination, CaR must be ubiquitinated at more than one lysine residue. All 16 lysine residues were therefore mutated to arginine simultaneously, and ubiquitination of the mutant, termed FLAG-CaR(0K), determined in the absence or presence of MG132 (Fig. 3*A*, *upper panel, lanes 3* and *4*). FLAG-CaR(0K) was not

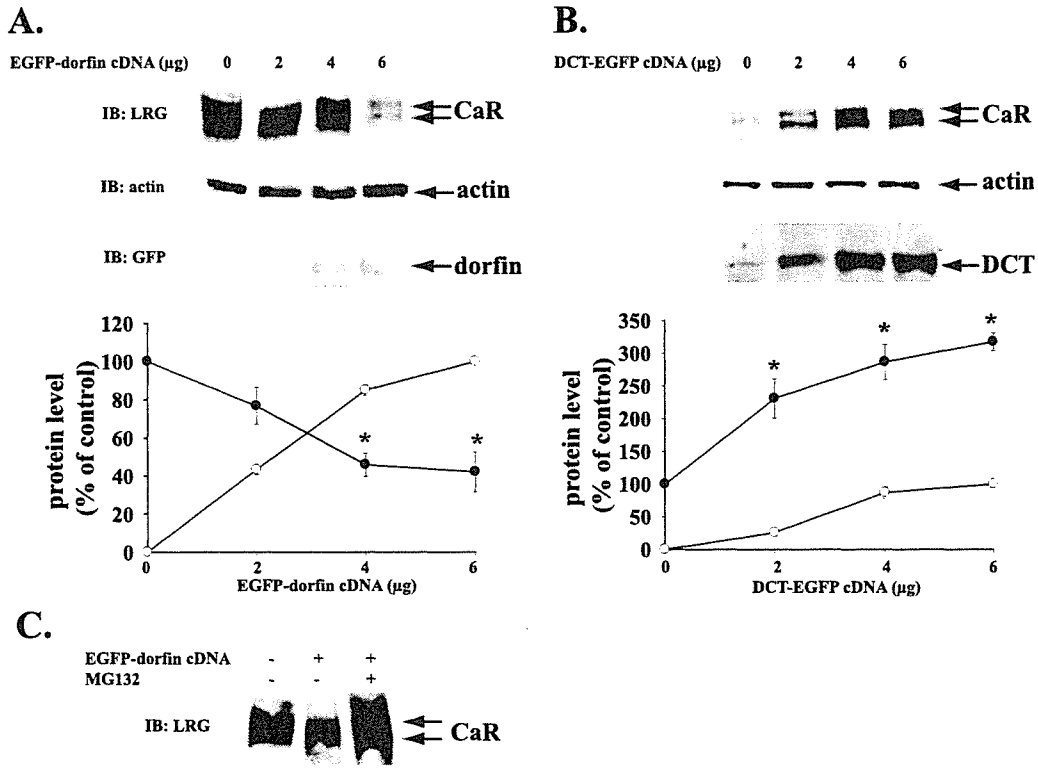

FIGURE 5. **Regulation of steady-state protein level of CaR by dorfin.** *A*, wild-type dorfin enhances degradation of CaR. FLAG-CaR cDNA (1 μg) was transfected into HEK293 cells with increasing amounts of EGFP-dorfin cDNA (0, 2, 4, or 6 μg). Cell lysates were probed for FLAG-CaR, endogenous actin, and EGFP-dorfin by immunoblotting (*IB*) with anti-CaR (*LRG*), anti-actin, or anti-GFP antibodies. Graph (average of three independent experiments) indicates normalized CaR protein or EGFP-dorfin as a function of transfected EGFP-dorfin cDNA. CaR protein was normalized to amount in the absence of exogenous EGFP-dorfin; EGFP-dorfin normalized to that observed at 6 μg of EGFP-dorfin cDNA. *Filled circles*, FLAG-CaR; *open circles*, EGFP-dorfin. *B*, dominant negative construct of dorfin (DCT-EGFP) stabilizes CaR. FLAG-CaR cDNA (1 μg) was transfected into HEK293 cells with increasing amounts of DCT-EGFP cDNA (0, 2, 4, or 6 μg). The remaining procedures were as described in *A*. Graph (average of three independent experiments) indicates normalized CaR protein or DCT-EGFP, normalized as described in *A*. *Filled circles*, FLAG-CaR; *open circles*, DCT-EGFP. For both *A* and *B*, significance was at $p < 0.05$ (*). *C*, FLAG-CaR cDNA (1 μg) was transfected into HEK293 cells without (*lane 1*) or with EGFP-dorfin (6 μg) (*lanes 2* and *3*). Cells were treated without (*lanes 1* and *2*) or with (*lane 3*) MG132 for 12 h before lysis. Cell lysates were probed for FLAG-CaR by immunoblotting with anti-CaR LRG antibody. *IP*, immunoprecipitate.

ubiquitinated to a significant extent even in the presence of MG132. In addition, the amount of FLAG-CaR(0K) was not significantly changed upon addition of MG132 (100% in the absence *versus* 107.6 ± 10.7% in the presence of MG132) (Fig. 3*A*, *lower panel*, *lanes 3* and *4*), whereas wild-type FLAG-CaR was sensitive to MG132 treatment (100% in the absence *versus* 148.4 ± 4.7% in the presence of MG132) (Fig. 3*A*, *lower panel*, *lanes 1* and *2*). Both FLAG-CaR and FLAG-CaR(0K) achieved mature glycosylation consistent with plasma membrane localization (Fig. 3*A*, *lower panel*) (6, 7) and had a comparable ability to stimulate ERK1/2 phosphorylation upon exposure of cells to 5 mM Ca^{2+} (Fig. 3*B*). The absence of FLAG-CaR(0K) ubiquitination is not the result of an inability to associate with dorfin, because immunoprecipitation with anti-FLAG antibody of either FLAG-CaR or FLAG-CaR(0K) results in coprecipitation of comparable levels of endogenous dorfin (Fig. 3*C*, *top panel*). Also illustrated in Fig. 3*C* is the presence of endogenous dorfin (*middle panel*) or transfected FLAG-CaR (*bottom panel*) in cell lysates. These results confirm that CaR is ubiquitinated at multiple lysine residues and degraded by the proteasome.

Dorfin Mediates CaR Ubiquitination—Dorfin is an E3 ubiquitin ligase and interacts with CaR and, therefore, likely mediates CaR ubiquitination. To test this possibility, FLAG-CaR and HA-Ub cDNAs were cotransfected into HEK293 cells, without or with EGFP-dorfin cDNA. Anti-FLAG antibody was used to immunoprecipitate CaR; Western blots were probed with anti-HA antibody to detect ubiquitinated species. In the absence of dorfin, a low level of CaR ubiquitination was detected; cotransfection with dorfin dramatically increased CaR ubiquitination (Fig. 4*A*). HEK293 cells express endogenous dorfin (data not shown, but see, *e.g.* Figs. 2*A* or 3*C*), and thus basal CaR ubiquitination (in the absence of cotransfected dorfin) might be catalyzed by endogenous dorfin. To test this possibility, we used DCT-EGFP as a dominant negative to interfere with ubiquitination mediated by endogenous dorfin. This construct cannot catalyze ubiquitination of substrates, because it does not contain the amino-terminal RING domains, which are essential for interaction with ubiquitin-conjugating enzymes (11). Cotransfection of HEK293 cells with FLAG-CaR, HA-Ub, and DCT-EGFP resulted in a reduction in CaR ubiquitination, compared with ubiquitination mediated by endogenous dorfin (-DCT) (Fig. 4*B*). These results suggest that the E3 ubiquitin ligase dorfin mediates ubiquitination of CaR.

Dorfin Regulates the Amount of CaR Protein in HEK293 Cells—Because dorfin mediates CaR ubiquitination, it must contribute to regulation of total cellular CaR protein. FLAG-CaR cDNA was transfected into HEK293 cells with increasing amounts of EGFP-dorfin cDNA (Fig. 5*A*). Total cDNA was kept constant with pcDNA3.1. The expression of CaR and dorfin were characterized by immunoblotting lysates from HEK293 cells with either anti-CaR LRG antibody (Fig. 5*A*, *top blot*) or anti-GFP antibody (Fig. 5*A*, *bottom blot*). Actin was used as a loading control (Fig. 5*A*, *middle blot*). When dorfin was increased, the amount of CaR decreased in a dose-dependent manner (Fig. 5*A*). The graph in Fig. 5*A* shows averaged results for three independent experiments and demonstrates a significant decrease in CaR protein as dorfin protein is increased.

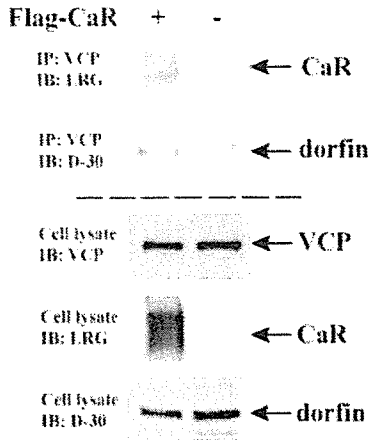

FIGURE 6. **VCP/CaR/dorfin coimmunoprecipitation in HEK293 cells.** HEK293 cells were transfected without (−) or with (+) FLAG-CaR cDNA. Cell lysates were immunoprecipitated (*IP*) with anti-VCP antibody, and Western blots were probed with anti-CaR antibody LRG (*first blot*). The same blot was stripped and reprobed with anti-dorfin antibody D-30 (*second blot*). The expression of endogenous VCP, transfected CaR, and endogenous dorfin were confirmed by immunoblotting (*IB*) cell lysates with anti-VCP antibody (*third blot*), anti-CaR LRG antibody (*fourth blot*), or anti-dorfin D-30 antibody (*fifth blot*).

When CaR cDNA was transfected into HEK293 cells with increasing amounts of the dominant negative DCT-EGFP cDNA, CaR protein in cell lysates increased as a function of DCT protein (Fig. 5*B*, *top blot*). The graph illustrates averaged results from three independent experiments (Fig. 5*B*). To confirm that EGFP made no contributions to the observed responses, a DCT construct containing a carboxyl-terminal c-*myc* epitope was also generated. DCT-c-*myc* protected CaR against dorfin-mediated degradation in a manner comparable to DCT-EGFP (data not shown), indicating that the dorfin fragment specifically competed with endogenous dorfin to protect against CaR degradation. These results suggest that endogenous dorfin regulates CaR degradation.

To test if dorfin mediates degradation of CaR in a proteasome-dependent manner, the effect of the proteasomal inhibitor MG132 on dorfin-mediated CaR degradation was examined. When cells cotransfected with FLAG-CaR and EGFP-dorfin were treated with MG132, the dorfin-dependent decrease of CaR protein level was abrogated (Fig. 5*C*), suggesting that a proteasome-dependent mechanism underlies dorfin-mediated degradation of CaR.

VCP Interacts with Both CaR and Dorfin—Dorfin interacts directly with VCP, an AAA-ATPase proposed to have a role in ERAD of proteins (14). In HEK293 cells transiently transfected with FLAG-CaR, an antibody against endogenous VCP immunoprecipitated both FLAG-CaR and endogenous dorfin (Fig. 6, *lane 1*). In the absence of FLAG-CaR, the anti-VCP antibody pulled down endogenous dorfin (Fig. 6, *lane 2*), as has previously been shown (14). Lower blots of Fig. 6 indicate endogenous expression of VCP and dorfin, as well as FLAG-CaR in lysates of transfected cells. Because both dorfin and CaR can interact with VCP, it is likely that dorfin-mediated ubiquitination and degradation of CaR is occurring at the ER via a VCP-facilitated ERAD pathway.

All Forms of CaR Are Degraded via the Proteasome—If CaR interacts with dorfin and VCP at the ER, it is possible that misfolded or unfolded, immature CaR is targeted for proteasomal degradation by dorfin. To test this possibility, we examined the effects of tunicamycin, an inhibitor of glucosaminyl 1-phosphate transferase, for the amounts and molecular weights of CaR in the absence or presence of MG132. Treatment with tunicamycin induced the appearance of unglycosylated CaR, with a molecular mass of 115 kDa (Fig. 7*A*). Two differentially glycosylated forms of CaR were also observed, *i.e.* bands at molecular masses of 130

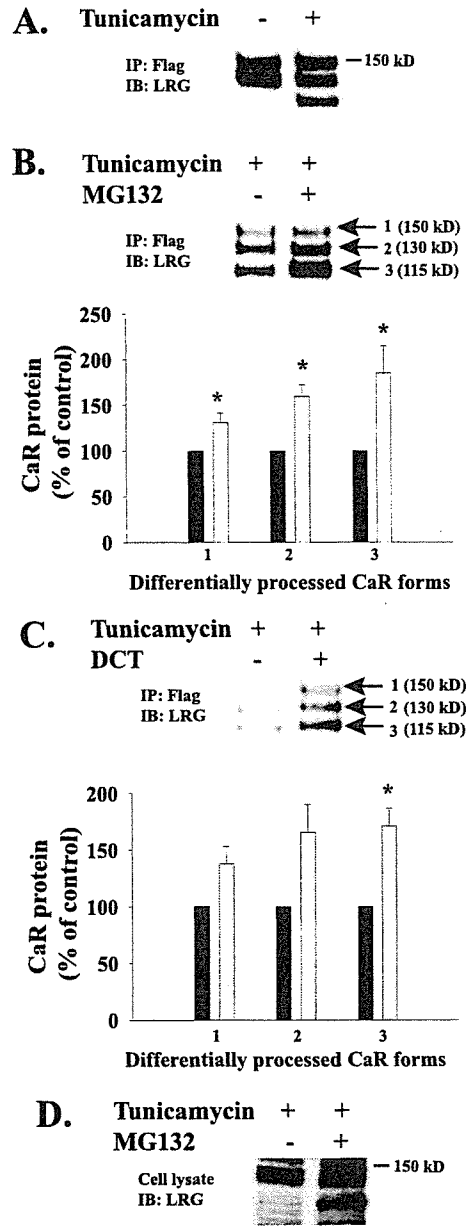

FIGURE 7. **Sensitivity of immature forms of CaR to proteasomal degradation.** *A*, tunicamycin stabilizes an immature form of CaR. HEK293 cells transfected with FLAG-CaR cDNA were treated without or with tunicamycin (5 μg/ml) for 12 h prior to lysis. Lysates were immunoprecipitated (*IP*) with anti-FLAG antibody and probed with anti-CaR LRG antibody. *B*, MG132 increases the amounts of immature forms of CaR. HEK293 cells were transfected with FLAG-CaR and HA-Ub cDNAs, and incubated with tunicamycin (5 μg/ml) without or with MG132 (10 μM), for 12 h prior to lysis. Lysates were immunoprecipitated with anti-FLAG antibody and probed with anti-CaR LRG antibody. Three forms of CaR are evident in tunicamycin: *1*, fully glycosylated CaR (150 kDa); *2*, ER-resident high mannose CaR (130 kDa); and *3*, unglycosylated CaR (115 kDa). The amount of CaR protein in each form was quantified in the absence or presence of MG132, and average results for three independent experiments are illustrated (each band normalized to the amount observed in the absence of MG132), significance was at $p < 0.05$ (*). *C*, DCT increases the amounts of immature forms of CaR. HEK293 cells were transfected with FLAG-CaR without or with DCT-EGFP. Cells were incubated with tunicamycin (5 mg/ml) for 12 h prior to lysis. Experiments were as in *A*. Graph indicates amounts of three forms of CaR protein in the absence or presence of DCT-EGFP, normalized to the amount in the absence of DCT-EGFP. Significance was at $p < 0.05$ (*). *D*, MG132 increases the amounts of immature CaR in MDCK cells. MDCK cells were treated with tunicamycin (5 μg/ml) without or with MG132 (10 μM) for 12 h prior to lysis. Lysates were immunoblotted (*IB*) with anti-CaR LRG antibody.